Precambrian Research 361 (2021) 106264

Contents lists available at ScienceDirect

Precambrian Research

journal homepage: www.elsevier.com/locate/precamres

Recognizing subsurface breccias in Archean terranes: Implications for district scale metallogeny

Marina D. Schofield [a,*], Harold.L. Gibson [a], Bruno Lafrance [a], K. Howard Poulsen [b], Jeffrey Marsh [a], Michael A. Hamilton [c], Taus R.C. Jørgensen [a]

[a] Metal Earth, Mineral Exploration Research Center, Harquail School of Earth Sciences, Laurentian University, 935 Ramsey Lake Road, Sudbury, Ontario P3E 2C6, Canada
[b] Consultant, 34 Wallford Way, Ottawa, Ontario K2E 6B6, Canada
[c] Jack Satterly Geochronology Laboratory, University of Toronto, 22 Russell Street, Toronto, Ontario M5S 3B1, Canada

ARTICLE INFO

Keywords:
Breccia
Magmatic-hydrothermal
VMS
Archean
Metallogeny

ABSTRACT

Breccias are common in ancient and modern volcanic terranes, where they form at and below surface through volcanic, hydrovolcanic, magmatic, or tectonic mechanisms. They are critical for volcanic reconstruction as stratigraphic markers and indicators of geodynamic change and since they can be associated with mineralization their genesis is also important from an exploration perspective. Their origin can be difficult to ascertain in ancient terranes that have undergone polyphase deformation and associated metamorphism. The Joliet Breccia is a subeconomic Cu-Ag prospect within the Neoarchean Rouyn-Noranda mining district, in the Abitbi greenstone belt, Canada. It was previously interpreted as a phreatic breccia formed on the seafloor. This study presents new data indicating that the Joliet Breccia is a subsurface magmatic-hydrothermal breccia. Specifically, the recognition of gradational contacts with host rocks and between internal breccia domains, lack of sedimentary features and the spatial and temporal association with a tonalite intrusion strongly supports this interpretation. The angular, poorly sorted, lithic clasts derived from the immediate host rocks, hydrothermal cement, complete absence of a rock flour matrix, and presence of a radial and concentric fracture pattern extending into the host rocks, further support a subsurface magmatic-hydrothermal emplacement mechanism.

A new TIMS U-Pb zircon age of 2698.0 ± 0.9 Ma (2σ) for a tonalite block within the breccia constrains the maximum age of brecciation. Four LA-ICP-MS U-Pb dates on hydrothermal monazite (2693.7 ± 1.0/8.9 Ma; 2696.9 ± 0.45/8.9 Ma; 2698.7 ± 1.4/8.9 Ma; 2701.2 ± 0.33/8.9 Ma; 2 $s/2s_{sys}$) found in the cement of the Breccia indicate brecciation and mineralization occurred shortly after the emplacement of the tonalite. Similarly, the ca. 2697 Ma St. Jude intrusive breccia indicates a localized ca. 2699–2695 Ma magmatic-hydrothermal event superimposed on ca. 2704–2701 Ma strata. These breccias are temporally correlative with the youngest units of the Blake River Group strata and associated ca. 2698–2695 Ma volcanogenic massive sulfide (VMS) deposits, which suggests an indirect genetic link between these two hydrothermal systems. The VMS deposits may represent the near surface, distal manifestations of a deeper magmatic-hydrothermal system akin to the porphyry-intermediate sulfidation epithermal continuum in modern subaerial volcanic arcs.

1. Introduction

Breccias are common to volcano-plutonic systems, and subsurface breccias are a frequent host to porphyry (e.g., El Teniente, Chile and Toquepala, Peru) and epithermal base and precious metal deposits (e.g., Red Mountain, Colorado; Pascua-Lama, Chile-Argentina; La Coipa, Chile; Wau, Papua New Guinea), making them preferred exploration targets because of their commonly high metal contents (Sillitoe, 1985; Sawkins, 1990). In addition, unique extrusive breccias serve as stratigraphic markers and provide insights into the changing dynamics of volcanic complexes, making their correct identification critical for volcanic reconstruction. In ancient volcanic successions, such as Precambrian greenstone belts, descriptions of subsurface breccias are rare, and there are few examples of mineralized breccias (e.g., Chadbourne, Québec, Walker and Cregheur, 1982; Newbec, Québec, Smith, 1983; Beidelman Bay intrusive complex, Ontario, Galley et al., 2000; St. Jude,

* Corresponding author.
E-mail address: mschofield@laurentian.ca (M.D. Schofield).

https://doi.org/10.1016/j.precamres.2021.106264
Received 3 December 2020; Received in revised form 27 April 2021; Accepted 2 May 2021
Available online 15 May 2021

Québec, Galley and van Breemen, 2002; Côté Au deposit, Ontario, Katz et al., 2017; Queylus, Québec, Mathieu and Racicot, 2019). The apparent paucity of subsurface breccias in ancient greenstone belts may, in part, be due to limited exposure and, in many cases, substantial deformation and alteration, making it difficult to distinguish subsurface versus surface emplacement.

The Joliet Breccia is hosted by ca. <2702–2699.5 Ma Blake River Group (McNicoll et al., 2014) strata of the Noranda volcanic complex and spatially associated with the past-producing Joliet Cu (Sabina, 2003) and Quemont Zn-Cu-Au-Ag massive sulfide deposits (Fig. 1). Since Wilson (1941), it has been interpreted as an extrusive steam explosion breccia, related to the emplacement of a quartz feldspar porphyritic rhyolite dike (Quemont feeder dike; De Rosen Spence, 1976; Lichtblau and Dimroth, 1980). Lichtblau and Dimroth (1980) expanded this interpretation and correlated the Joliet Breccia to the host <2702–2699.5 Ma strata, in particular to a proximal volcaniclastic unit referred to as the "upper marker horizon", emphasizing a genesis at the seafloor. Their model interpreted layering in the Joliet Breccia to be bedding and they interpreted the tonalite blocks as an intact and unrelated younger intrusion. However, their observations do not preclude a subsurface emplacement mechanism for the Joliet Breccia and similarities to younger (ca. 2698 Ma) discordant mineralized breccia bodies within the Rouyn-Noranda mining district (Fig. 1) were not considered.

This study presents results of new detailed mapping, petrography, geochemistry and geochronology to unravel the timing, emplacement mechanism, and origin of the Joliet Breccia and its associated mineralization within the context of the broader metallogeny of the Rouyn-Noranda mining district. We explore the temporal relationship between the Joliet Breccia and other intrusive breccias, and with the volcanism and plutonism that constructed the Noranda volcanic complex and associated ore deposits. Ultimately, using the Joliet Breccia as a type example, we present criteria that aid distinguishing surface and subsurface breccias in ancient terranes, which has significant ramifications for volcanic reconstruction and exploration.

2. Geological setting of the Joliet Breccia

The Rouyn-Noranda mining district is located within the Blake River Group of the southern Abitibi greenstone belt of the Superior Province (Fig. 1). Volcanic rocks of the district comprise the Noranda Subgroup (De Rosen Spence, 1976; Goodwin, 1980), a 6000 m thick bimodal volcanic complex of the Blake River Group (Fig. 1), which was constructed over a 7 m.y. period (McNicoll et al. 2014). The Noranda Subgroup was subdivided into informal lithostratigraphic formations (De Rosen Spence, 1976; Gibson, 1990) and subsequently into informal chronostratigraphic "formations" by McNicoll et al. (2014). McNicoll et al. (2014) recognized a regional time gap in Noranda Subgroup volcanism at 2700–2698.5 Ma, with VMS deposits occurring in strata older (e.g., Horne, Quemont deposits) and younger (Bouchard-Hebert deposit) than this break. The Joliet Breccia is located in older ca. 2702–2699.5 Ma volcanic strata of

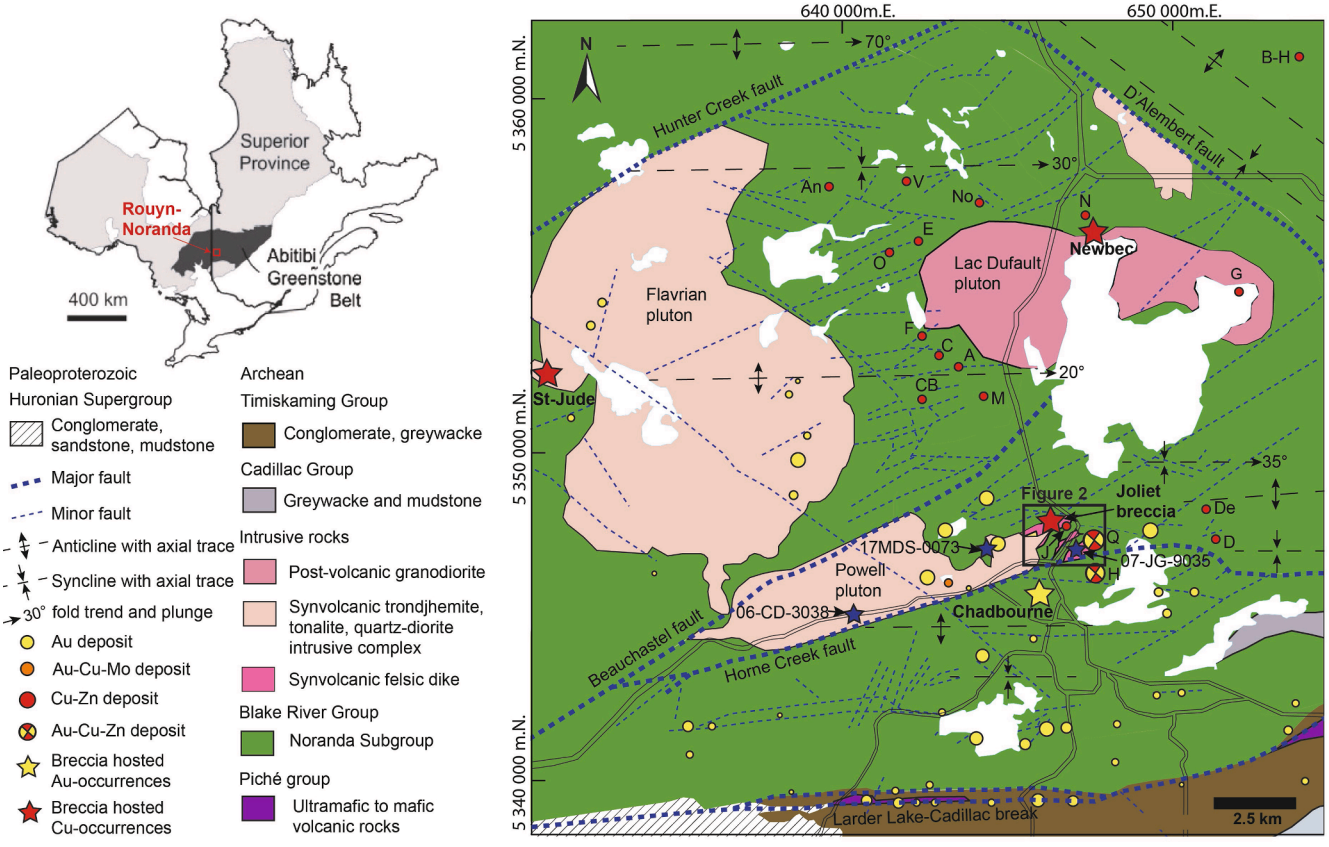

Fig. 1. Regional map of the Noranda volcanic complex, modified from Poulsen (2017) and McNicoll et al. (2014). The Noranda volcanic complex comprises the Noranda Subgroup (De Rosen Spence, 1976; Goodwin, 1980) of the Blake River Group. The Noranda Subgroup represents 7 m.y. of continuous volcanism except for a distinct break in volcanism between 2700 and 2698.5 Ma with VMS deposits occurring in volcanic strata older and younger than this break. The locations of discordant breccia bodies are shown by red and yellow stars; the colour reflects the dominance of copper or gold respectively. Blue stars show the location of previously reported U-Pb ages in the Powell Block, which is the wedge shaped fault block bound to the north by the Beauchastel fault and to the south by the Horne Creek fault. Axial traces of regional synclines and anticlines from Hubert et al. (1984). VMS and orogenic gold deposits are shown by red and yellow circles respectively. The yellow circles are scaled to reflect the relative gold tonnage. (An = Ansil, V = Vauze, No = Norbec, N = Newbec, B-H = Bouchard-Hebert, O = Old Waite, E = East Waite, G = Gallen, F = Amulet F, C = Amulet C, A = Amulet A, CB = Corbet, M = Millenbach, J = Joliet, De = Deldona, D = Delbridge, Q = Quemont, H = Horne).

the Powell Block (Fig. 1). The region has undergone four increments of deformation, the greatest strain related to north–south shortening that occurred <2669–>2639 Ma (Dubé and Mercier-Langevin, 2020), and folded the volcanic strata into a series of open, gently east-plunging anticlines and synclines, and an associated axial planar E-W cleavage (Goulet, 1978; Dimroth et al., 1983; Hubert et al., 1984; Wilkinson et al., 1999; Bedeaux et al., 2017; Poulsen, 2017).

The Joliet Breccia occurs along the northern margin of the northernmost Quemont feeder dike, one of three ENE trending, quartz-feldspar-porphyritic rhyolite intrusions (Fig. 2), which are interpreted to be feeder dikes to a quartz-feldspar-porphyritic rhyolite flow that comprises the hanging wall to the Quemont VMS deposit (De Rosen Spence, 1976; Lichtblau, 1989; McNicoll et al., 2014). The dikes also cross-cut northwesterly-striking volcanic rocks of the Joliet formation (De Rosen Spence, 1976).

The northernmost dike is approximately 350 m wide, has a strike length of 1300 m, dips steeply to the north at 85° and contains ~5% quartz (0.5–1 mm) and 1% plagioclase phenocrysts (0.5–1 mm). The southernmost dike, which is compositionally, mineralogically and texturally similar yielded a ca. 2702.0 ± 0.8 Ma U-Pb zircon age (07-JG-9035; McNicoll et al., 2014). McNicoll et al. (2014) defined this sample as the extrusive Quemont rhyolite flow, however the contact relationships are not exposed, and this sample was taken from an area denoted to be the intrusive Quemont feeder dike by De Rosen Spence (1976). Sample 18MDS-0107 (Fig. 3) of the northernmost dike, collected for this study, did not yield zircon grains; however, the three feeder dikes are interpreted to be the same age and a product of the same volcanic event (De Rosen Spence, 1976; Lichtblau and Dimroth, 1980; Lichtblau, 1989; McNicoll et al., 2014).

To the southwest, the Quemont feeder dikes are cross-cut by the Powell tonalite of the composite Flavrian-Powell Intrusive Complex (Fig. 2). Smaller tonalite intrusions locally cross-cut the Quemont feeder dike and one in particular coincides with the Joliet Breccia, and is henceforth referred to as the "Joliet tonalite". The northernmost Quemont feeder dike marks a significant synvolcanic fault (Fig. 2) that separates andesites of the Powell formation to the north from rhyolite flows of the Joliet formation to the south (De Rosen Spence, 1976; Lichtblau, 1989). Volcanic strata of the Powell formation strike WNW, dip ~80° east and consist of massive amygdaloidal andesite, overlain by a conformable mafic volcaniclastic unit referred to as the "upper marker horizon" by Lichtblau (1989), herein referred to as the upper marker unit. The contact between the andesite and the Quemont feeder dike is sharp, irregular, and discordant. The contact between the Joliet Breccia and the upper marker unit is not exposed. The upper marker unit is conformably overlain by massive andesite. East-northeast striking, boudinaged, aphyric rhyolite dikes oriented subparallel to the Quemont feeder dike, cross-cut the andesite (Fig. 3).

Volcanic strata south of the northernmost dike (Fig. 2) consist of the aphyric, coherent to brecciated rhyolite of the Joliet formation, which is host to the Joliet Cu-deposit, and is conformably overlain by crudely bedded, polymictic volcaniclastic units of the Quemont formation (Lichtblau, 1989). The gold-rich Quemont VMS deposit occurs at the contact between the Joliet formation and the Quemont formation, southeast of the Joliet Breccia (Fig. 2). The contact between the Joliet formation and northernmost Quemont feeder dike is sharp and discordant.

An E-W striking, moderately dipping cleavage cross-cuts all units within the map area (Hubert et al., 1984), including the Joliet Breccia. This is parallel to the main foliation observed elsewhere within the Rouyn-Noranda mining district that is commonly axial planar to E-W trending folds and is related to a north–south shortening event, which is interpreted as broadly coeval with the main regional dynamothermal metamorphic planar fabric which affects the Blake River Group volcanic rocks and younger Timiskaming Group sedimentary rocks (Fig. 1) at Noranda and elsewhere implying that it formed after 2669 Ma, the maximum age for Timiskaming deposition (Wilkinson et al., 1999; Bedeaux et al., 2017; Poulsen, 2017).

Cross-cutting relationships and the established age of deformation constrains formation of the Joliet Breccia between ca. 2702.0 ± 0.8 Ma and >2669 Ma. This approximately 34-million-year window questions whether the Joliet Breccia timing is related to early Blake River Group volcanism or to early post-Timiskaming deformation, as previously interpreted for the Chadbourne breccia (Walker and Cregheur, 1982) or alternatively to intervening geological events.

3. Methodology

Detailed mapping was conducted over the span of two months aided by high resolution digital aerial photos at 1:500 scale and compiled at 1:2000 scale. Petrography was completed on polished slabs and on polished thin sections through standard transmitted and reflected light microscopy. Mineralogy was verified using the Scanning Electron Microscope (SEM) and energy-dispersive spectroscopy (EDS) at the Mineral Exploration Research Centre Isotope Geochemistry Laboratory of Laurentian University. High precision isotope-dilution – thermal ionization mass spectrometry (ID-TIMS) U-Pb zircon geochronology was completed at the Jack Satterly Geochronology Laboratory, University of Toronto. Laser ablation Inductively Coupled Mass Spectrometry (LA-ICPMS) U-Pb monazite geochronology was completed at the MERC Isotope Geochemistry Laboratory of Laurentian University. Details of analytical setup and results are provided in supplementary data file 1 and file 2, respectively. Samples were submitted to ALS Geochemistry, in Sudbury, Ontario for crushing, pulverising and whole-rock geochemical analysis. Detailed description of all methodologies used can be found in supplementary data file 1. Results for the 53 analyzed samples for the metal zonation study are provided in supplementary data file 3. Whole rock data for the 25 analyzed samples used for lithological and alteration characterization are provided in supplementary data file 4.

4. Results

4.1. Description of the Joliet Breccia

The Joliet Breccia is 250 m by 150 m in area, has a crude, elliptical form (Fig. 3), straddles the contact between the Quemont feeder dike and the upper marker unit, and encompasses several masses composed of intact tonalite. Based on the relative abundance of felsic and mafic clasts the Joliet Breccia is divisible into three WSW striking domains: felsic, transitional and mafic. The three domains do not have an annular distribution within the Joliet Breccia, but reflect their immediate host rocks and show a south to north progression from felsic to transitional to mafic dominated clast domains, which terminate against the host Quemont feeder dike and the upper marker unit to the north (Fig. 3). Internal domain contacts and the contact between the breccia and the host rocks are gradational. The breccia noticeably lacks sedimentary features such as bedding. Clasts within all domains are poorly size-sorted and have distinctly angular, rectangular to tabular shapes with curviplanar margins. They are commonly oriented with their long axis parallel to the internal contacts between domains. The breccia is typically clast supported with a cement (10–20%) comprising prismatic comb textured quartz (3–5 mm long) ± acicular Fe-chlorite rosettes ± sulfides (Fig. 4A) that grew syntaxially from clast margins. There is no evidence of a finer clastic, or rock-flour matrix component.

The outer limit of the Joliet Breccia is defined by an asymmetrically developed, 6 m wide zone of altered conjugate fractures containing localized areas of *in situ* breccia within the Quemont feeder dike and upper marker unit (Fig. 3). The *in situ* breccia reflects an inward and progressive increase in void space marked by an increase in quartz infill along the conjugate fractures grading into localized areas of monomictic, jig-saw fit breccia, wherein tabular clasts of the host Quemont feeder dike are rotated and clast margins mirror the orientation of the conjugate fractures. The contact between *in situ* brecciated Quemont feeder dike and the felsic dominated domain of the Joliet

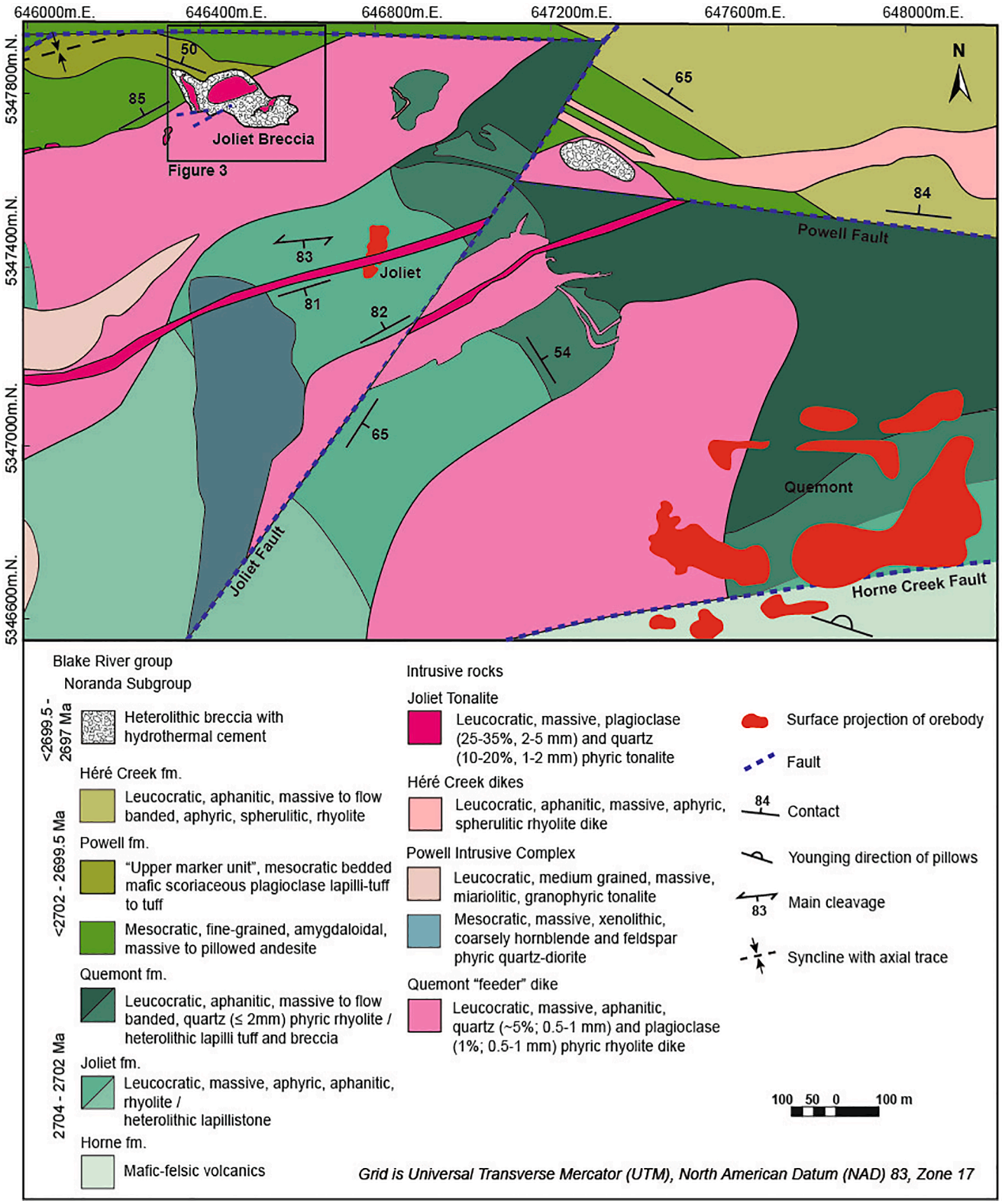

Fig. 2. Local geology map from rectangle outlined in Fig. 1 showing the distribution of mineral deposits within the Joliet Breccia area. Orebodies are vertical surface projections. Modified from Morris (1957, 1959), De Rosen Spence (1976), and Joliet-Quebec Mines Ltd. (1948). Original informal lithostratigraphic formations of De Rosen Spence (1976), shown as shades of green or blue to correspond to the informal chronostratigraphic divisions of McNicoll et al. (2014). Proterozoic diabase dikes are present in the map area but were omitted for clarity.

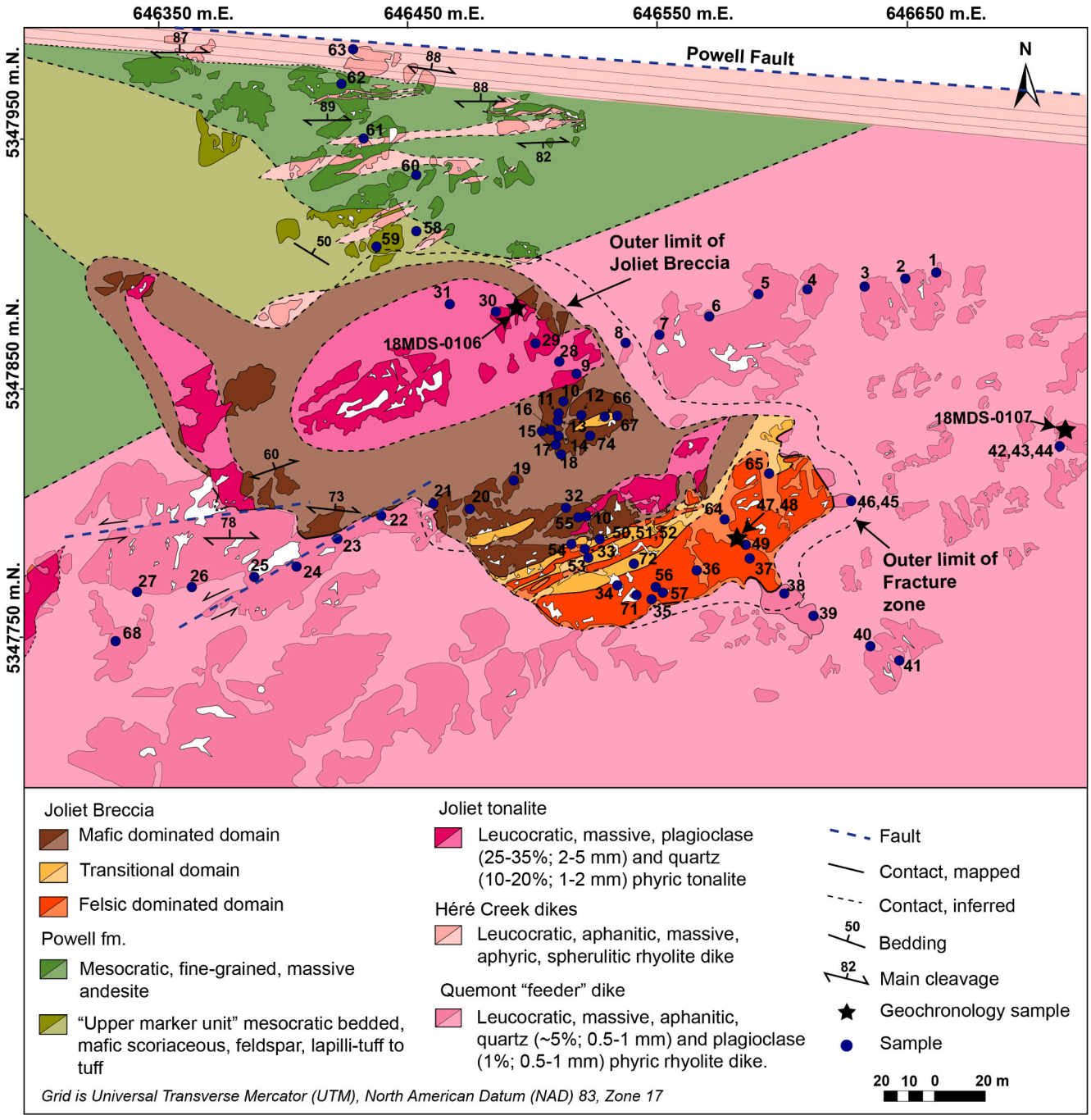

Fig. 3. Geological map of the Joliet Breccia. Outcrop exposures are outlined; white patches denote areas covered by overburden. Lighter shades for each lithology show interpolation between outcrop exposures. The northwestern margin of the Joliet Breccia is poorly defined due to lack of outcrop exposure. Thin parallel lines within the Powell fault denote a zone of high strain and indicates the orientation of the shear fabric. Sample traverses for metal zonation are shown by blue dots. Samples collected for U-Pb TIMS geochronology are shown by black stars.

Breccia is gradational and defined by the first appearance of breccia with quartz infilled open void space >10% by area. The felsic dominated domain of the Joliet Breccia is a monomictic, jig-saw fit breccia containing >70% quartz-feldspar porphyritic rhyolite clasts of the host Quemont feeder dike that range in size from generally 1–70 cm, with rare blocks up to 2–3 m diameter (Fig. 4B). The cement is dominantly quartz (Fig. 4C), with a gradational increase in interstitial chlorite that imparts an angular patchy morphology (Fig. 4D) towards the WNW in proximity to the transitional domain. The quartz-feldspar porphyritic rhyolite clasts have distinctive white silicified rims where associated with chlorite cement (Fig. 4D).

The transitional domain (Fig. 4E) is a polymictic breccia containing 40–60% pervasively chloritized and locally spotted mafic clasts and ≤60% quartz-feldspar porphyritic rhyolite clasts. Thin, west-southwest trending septa or lenses of the felsic dominated domain occur within the transitional domain; the contacts between these domains are parallel to the strike of the Quemont feeder dike (Fig. 3). Relative to the felsic dominated domain, clasts within the transitional domain are rotated, more equant and rectangular in form, and are smaller, with an average clast size of 5–14 cm.

The mafic dominated domain is a polymictic breccia containing >60% mafic clasts (Fig. 4F). Clasts range in size from 3 to 60 cm, with

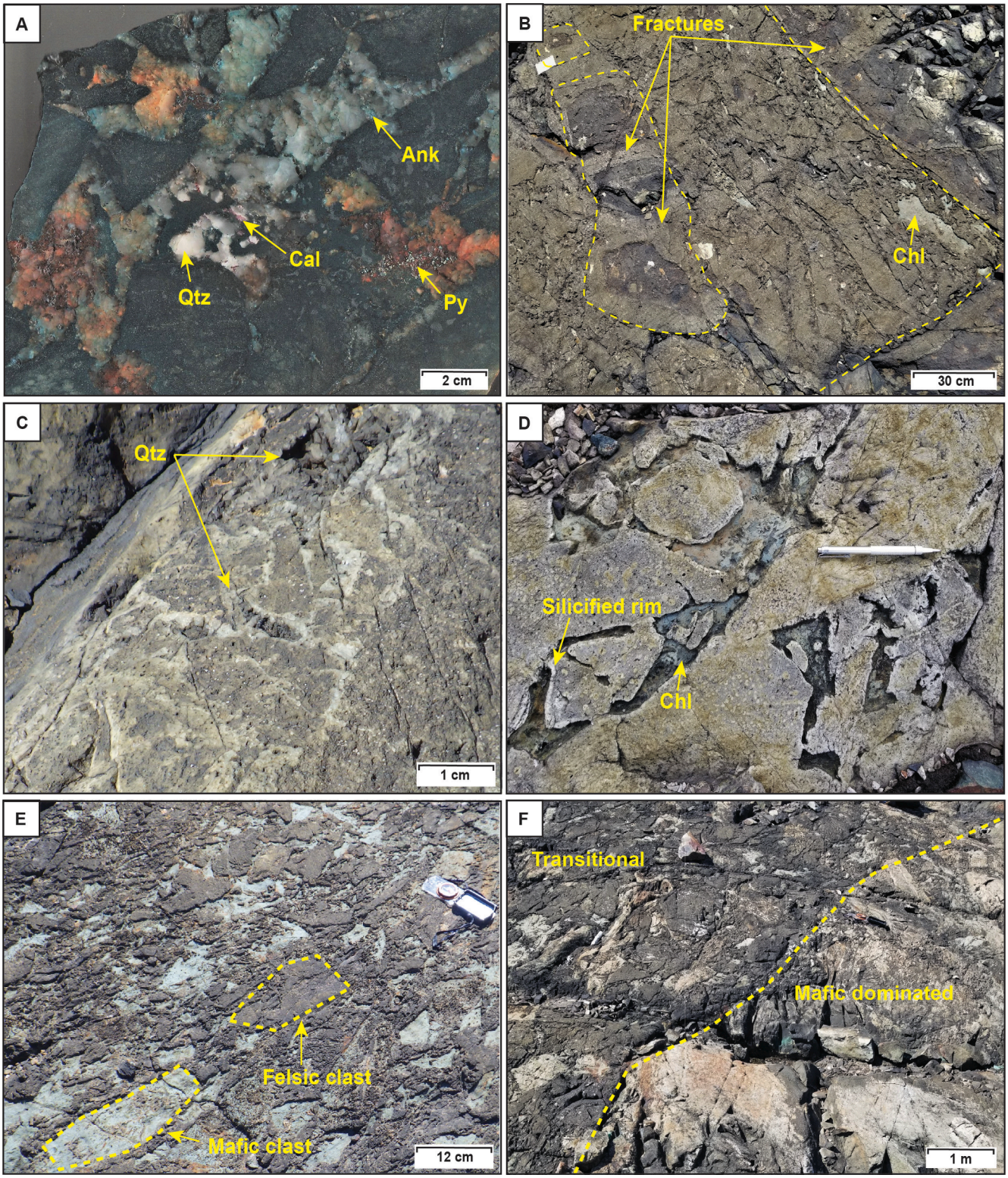

Fig. 4(A-F). A) Mafic dominated domain of the Joliet Breccia. Note, angular tabular chlorite altered mafic fragments and a cement of white comb quartz, calcite, ankerite and pyrite. Ankerite is stained turquoise and calcite is stained pink following the method of Hitzman (1999) (polished stained slab); B) Felsic dominated domain of the Joliet Breccia. Note, jig-saw fit and elongate form of clasts, pervasive sericitization of smaller clasts, and larger blocks with internal fractures that are parallel to clast boundaries, with sericite alteration haloes that do not cross-cut the breccia (field photograph); C) Euhedral, pyramidal quartz cement, between in-situ, jig-saw fit clasts of the felsic dominated domain (field photograph); D) Chlorite cement within the felsic dominated domain. Note, the white silicified clast rims (field photograph); E) Transitional domain showing mafic and felsic clasts (field photograph); F) Contact between the transitional domain and the mafic dominated domain (field photograph). (Ank = ankerite, Cal = calcite, Chl = chlorite, Py = pyrite, Qtz = quartz).

local blocks >2 m. Thin, west-southwest trending septa or lenses of the transitional domain occur within the southern part of the mafic dominated domain; their orientation is parallel to the strike of the Quemont feeder dike. The five felsic clast types are representative of adjacent host rocks and include: i) quartz-feldspar porphyritic rhyolite clasts of the Quemont feeder dike; ii) clasts of the felsic dominated domain (jig-saw fit-texture of quartz-feldspar porphyritic rhyolite clasts separated by vuggy quartz; Fig. 4G); iii) silicified spherulitic, quartz microporphyritic rhyolite (≤1 mm, ~1% quartz); iv) aphyric-aphanitic rhyolite, identical to aphyric felsic dikes within the adjacent host rocks; and v) medium-grained tonalite (Fig. 4H). The five mafic clasts types are identical to the host volcanic strata and include: i) aphanitic to fine-grained massive andesite (Fig. 4H); ii) amygdaloidal (10%, 0.5–5 cm diameter amygdales) massive andesite; iii) plagioclase-phyric massive andesite; IV) plagioclase crystal lapilli-tuff (upper marker unit), consisting of scoriaceous plagioclase-phyric clasts in a matrix of plagioclase crystals and fine, ash-sized material with chloritized sideromelane shards; and V) blocks of finely bedded mafic tuff. The contact between the mafic dominated domain and the upper marker unit is not exposed, but conjugate fractures are recognized in one outcrop of the upper marker unit immediately adjacent to the Joliet Breccia.

Large tonalite blocks, within the mafic dominated domain, range in size from decimetres (Fig. 4H) to 40 m × 25 m mega blocks. The outcrop pattern for the tonalite megablocks (Fig. 3) suggest they are remnants of a tonalite dike or plug; contacts with the surrounding mafic dominated breccia are not chilled (Fig. 4I) and are marked by broken quartz crystals within the tonalite (Fig. 4J). The tonalite is equigranular to porphyritic, consisting of 40–50% medium-grained quartz and altered albite phenocrysts within a fine-grained spherulitic groundmass (50–60%) of quartz, albite, sericite and chlorite. Phenocrysts have distinctive, fine-grained, spherulitic coronas defined by radiating quartz, sericite and altered albite (Fig. 4K). Quartz phenocrysts (10–20%, 1–2 mm) are euhedral to subhedral and smokey grey in colour. Albite phenocrysts (25–35%, 2–5 mm) are subhedral to euhedral tabular crystals that are intensely altered to sericite, but preserve remnant polysynthetic twinning. The groundmass is a fine-grained mosaic of quartz and albite ± fine-grained euhedral pyrite (1–3%), cross-cut by arcuate perlitic fractures altered to sericite ± chlorite. The groundmass mosaic comprises spherulites showing all degrees of recrystallization from sector recrystallized spherulites (Fig. 4L) to quartz grains with irregular to rounded (anhedral) outlines and containing internal radiating feldspar laths. The tonalite contains irregular, chloritized, quartz-porphyritic xenoliths.

4.2. Lithogeochemistry

Whole-rock major and trace element analytical data from the Joliet tonalite, Quemont feeder dike and the Powell tonalite share similar geochemical characteristics. They plot as rhyodacite/dacite in the Pearce (1996) classification diagram (Fig. 5A), exhibit relatively flat chondrite-normalized REE patterns (La/Yb ratios 3–5), low Zr/Y ratios of 4–7, distinct negative Nb and Ti anomalies (Fig. 5B), have a transitional to calc-alkaline affinity (Fig. 5C), and are classified chemically as FIIIa/FIV rhyolites (Fig. 5D) (Hart et al., 2004). The mafic, chloritized clasts have a calc-alkaline affinity (Fig. 5C), and are basaltic in composition (Fig. 5A) with Zr/Y ratios of 5–7.5 and Y values of 20–30 ppm. The mafic clasts have negative Nb and Ti, anomalies and a relatively flat REE pattern (Fig. 5B) identical to the andesitic rocks of the Powell formation.

4.3. Zircon U-Pb ID-TIMS geochronology

Two samples were selected for U-Pb ID-TIMS analysis to provide a better temporal constraint on magmatism within the Powell Block. A sample of the eastern Powell tonalite (17MDS-0073; Fig. 1) that cross-cuts the northernmost Quemont feeder dike yielded a zircon population comprising irregular, cracked, broken, and rarely elongate forms generally lacking well-developed crystal faces (Fig. 6A). Chemical abrasion and subsequent analysis of the three clearest single grains from this population overlap with each other and Concordia, and gives a weighted average $^{207}Pb/^{206}Pb$ age of 2701.0 ± 0.8 Ma with good fit (MSWD = 0.90; Fig. 6A, Table 1). This new age is within 2σ error of a 2700.1 ± 1.0 Ma U-Pb zircon age obtained by McNicoll et al. (2014) for the lower Powell trondjhemite located to the southwest (06-CD-3038; Fig. 1) and is interpreted as the crystallization age for the Powell tonalite.

Sample 18MDS-0106 was collected from the largest tonalite megablock within the Joliet Breccia (Fig. 3). This sample yielded a robust population of clear and colourless, well faceted, stubby to elongate prismatic zircon grains (Fig. 6B). Analyses for three single, subequant to broken elongate euhedral crystals gave concordant to slightly discordant (1.5%) results, with a relatively narrow range of overlapping model $^{207}Pb/^{206}Pb$ ages between 2697.5 and 2699.2 Ma (Table 1). A regression of the data, anchored at the origin, yields an age of 2698.0 ± 0.9 Ma (2σ; MSWD = 1.19; Fig. 6B), which is interpreted as the age of igneous crystallization of the tonalite block within the Joliet Breccia. This indicates that the Joliet tonalite is demonstrably younger than the Powell tonalite, and constrains a maximum age of formation for the Joliet Breccia.

4.4. Structural analysis

The host rocks of the Joliet Breccia are cross-cut by a conjugate set of fractures that are oriented radial and concentric to the breccia within 6 m of the latter (Fig. 7). The fractures exhibit 15–60 cm spacing and are best developed along the ESE margin of the Joliet Breccia. They are ~1 mm wide, locally infilled by quartz ± sulfides, and are enveloped by the mineral association muscovite-quartz typical of sericite alteration (~4–8 cm wide), which is more resistant to weathering than the less altered host rock. Quartz within the fractures displays a euhedral comb habit oriented perpendicular to fracture walls. The mean orientation of the line of intersection between the fracture sets, as calculated using the Fisher analysis tool in Stereonet 10.0® (Allmendinger et al., 2012), is sub-vertical, plunging 88° towards 137° (Fig. 7). The main regional E-W striking cleavage overprints the sericite-quartz alteration halos of the fracture sets and all rock types within the area. In addition, jogs in the breccia's outer contact correspond to minor sinistral fault offsets (Fig. 7).

4.5. Mineralization

Sulfide minerals occur in the hydrothermal cement of the Joliet Breccia (Fig. 8A-B) and, to a lesser extent, in local cross-cutting fractures (Fig. 8C). The dominant sulfide phases, in order of decreasing modal abundance, are pyrite, chalcopyrite and pyrrhotite.

4.5.1. Hydrothermal cement

White, coarse-grained comb quartz ± fibrous Fe-rich chlorite ± fibrous muscovite is the dominant hydrothermal cement of the Joliet Breccia, whereas sulfide minerals within vugs are spatially restricted and asymmetrically distributed (Fig. 8D). Pyrite occurs as euhedral to subhedral (0.5–4 mm) grains intergrown with comb quartz (Fig. 8D-E). Comb quartz crystals are fractured and overgrown by a finer grained, polygonal mosaic of grey quartz (Fig. 8E-F). Syn-deformational fringe structures occur around some pyrite grains within the quartz mosaic (Fig. 8E). Both generations of quartz exhibit undulose extinction, indicating some internal deformation, and have recrystallized grain boundaries (Fig. 8G). The distribution of the grey quartz mosaic is asymmetric with respect to the vug margins and locally cross-cuts comb quartz (Fig. 8F). Chalcopyrite and pyrrhotite typically occur intergrown with and interstitial to the polygonal grey-quartz as anhedral clusters ~0.1–1 mm in diameter (Fig. 8F-I). Where pyrite occurs with chalcopyrite it is corroded and fractured with numerous fine-grained inclusions and veinlets of chalcopyrite (Fig. 8I). Locally, sulfides are associated with ferroan dolomite and/or calcite (Figs. 4B and 8J) that cross-cuts clasts

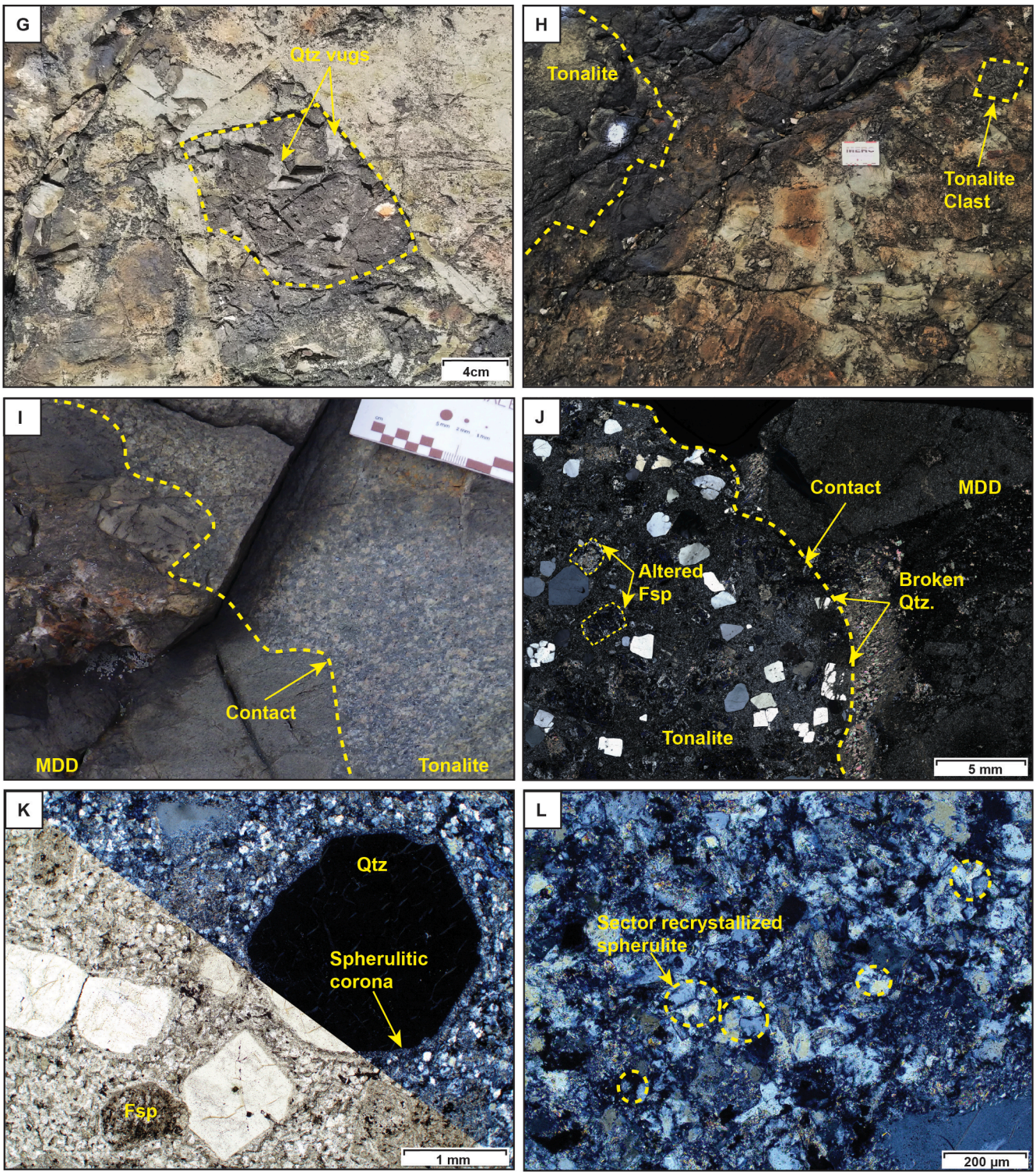

Fig. 4(G-L). G) Large block of the felsic-dominated domain in the mafic-dominated domain. Note the internal jig saw fit texture of monomictic quartz-porphyritic blocks separated by vuggy quartz, which is truncated by chlorite cement of the host mafic dominated domain (field photograph); H) Angular, tabular blocks of tonalite and andesite, within the mafic-dominated domain (field photograph); I) Intact Joliet tonalite in contact with the mafic-dominated domain; note the difference in grain size and abundance of quartz phenocrysts relative to the Quemont feeder dike. Numerous altered albite phenocrysts shown as white tabular grains display fuzzy, diffuse margins. Sharp, non-chilled, contact between the tonalite and mafic dominated domain (field photograph); J) Broken quartz crystals within Joliet tonalite at contact with mafic dominated domain (cross-polarized light); K) Joliet tonalite showing quartz and altered albite phenocrysts within an aphanitic, spherulitic groundmass (cross-polarized light (top right)/transmitted light (bottom left)). Note, spherulitic coronas surrounding phenocrysts; L) Spherulitic groundmass of the Joliet tonalite, showing sector recrystallized spherulites (cross-polarized light). (Fsp = feldspar, MDD = mafic dominated domain, Qtz = quartz).

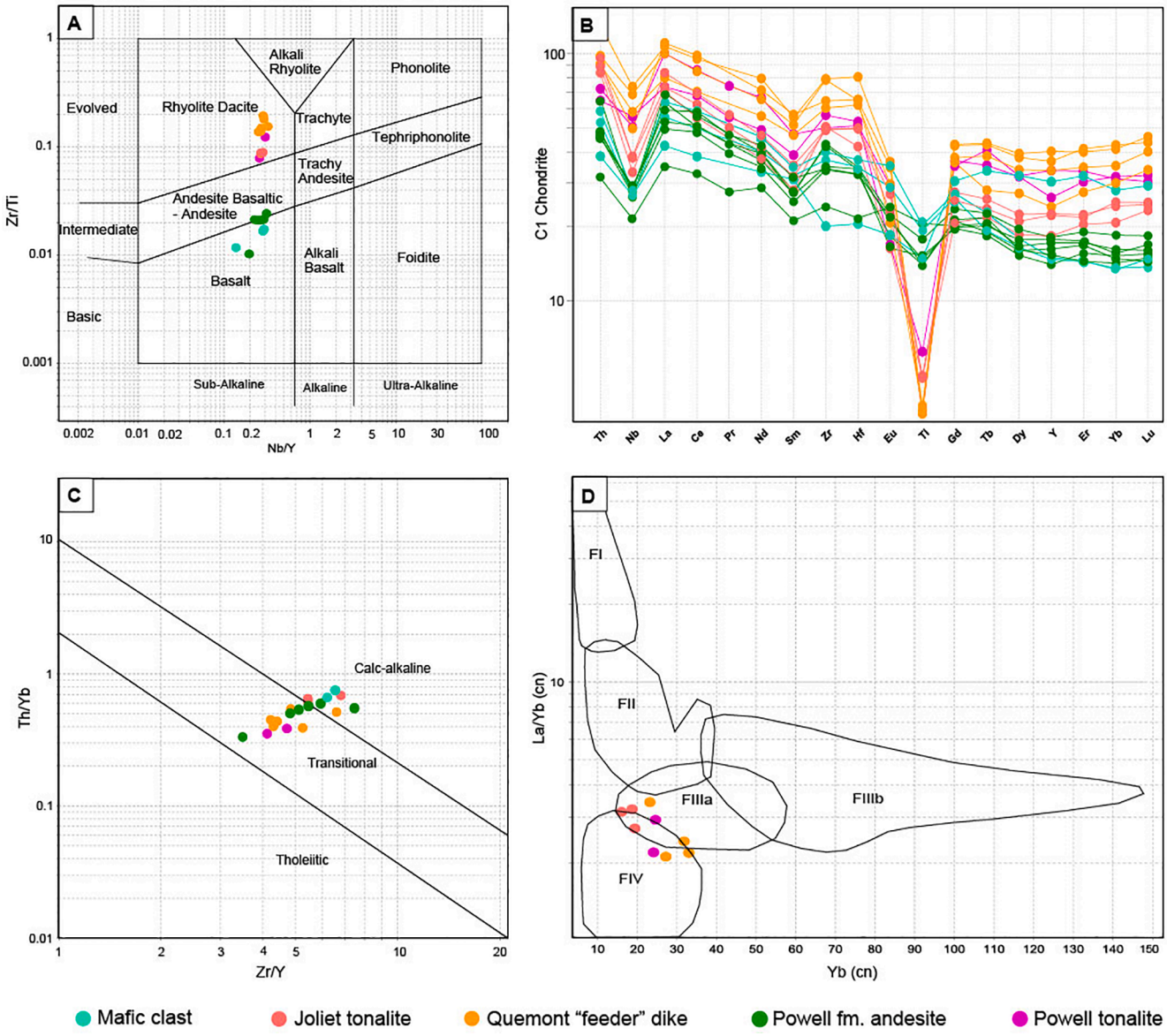

Fig. 5. Geochemical classification of the main lithologies. A) Volcanic rock classification (Pearce, 1996); B) Spider diagram, chondrite normalized immobile trace elements (Sun and McDonough, 1989); C) Magma associations determined by Zr/Y vs Th/Yb ratios (Ross and Bédard, 2009); D) Rhyolite fertility classification (Hart et al., 2004).

and vugs and infills remaining void space within vugs. In addition, all sulfides typically have red hematite rims (Fig. 8K), which imparts a red stained appearance to associated quartz (Fig. 8B). Other accessory phases include euhedral to subhedral apatite (~20–50 μm), fibrous to bladed rutile (~20–100 μm in length) and subhedral monazite (~0.02–1 mm) (Fig. 8K). Silver and Bi tellurides occur as anhedral clusters (~20–80 μm in diameter) interstitial to and intergrown with chlorite and along microfractures (Fig. 8L). The Ag and Bi telluride clusters are zoned and consist of an outer rim of hessite (Ag_2Te), followed by coarser laths of tetradymite (Bi_2Te_2S) that generally point inward toward a wormy intergrowth core of hessite and galena.

4.5.2. *Monazite U-Pb LA-ICP-MS geochronology*

Monazite grains (0.01–1 mm) in two Joliet Breccia samples of mineralized chlorite filled vugs (e.g., Fig. 8K) within the felsic-dominated domain were analyzed *in situ* by LA-ICPMS. Full details of the methodology, U-Pb geochronology and trace element data are presented in supplementary data files 1 and 2, with the compiled data summarized here. Full propagation of systematic uncertainties following the method of Horstwood et al. (2016), including the uncertainty in the primary reference material age and the long-term variance in the verification reference material dates, yields true uncertainties ($2S_{sys}$) for each weighted mean age of 8.9 Ma. The two largest monazite grains from sample 48 (Fig. 9A and B) yielded weighted mean $^{207}Pb/^{206}Pb$ ages of 2696.9 ± 0.45/8.9 Ma (Fig. 9D; 2 $s/2s_{sys}$; MSWD = 0.45; n = 120/134) and 2701.2 ± 0.33/8.9 Ma (Fig. 9E; 2 $s/2s_{sys}$; MSWD = 0.71; n = 409/431). Sixteen smaller grains from two sections of sample 47 yielded weighted means of 2693.7 ± 1.0/8.9 Ma (Fig. 9F; 2 $s/2s_{sys}$; MSWD = 1.09; n = 42/50; 10 grains) and 2698.7 ± 1.4/8.9 Ma (Fig. 9G; 2 $s/2s_{sys}$; MSWD = 2.5; n = 47/61; 6 grains), for each section respectively. A small percentage of analyses were >5% discordant outside of 2σ of the mean, representing younger (<~2670 Ma) or older (>~2710 Ma), and were excluded from the weighted mean calculations (see supplementary data file 1). These ages indicate that brecciation and mineralization occurred between 2701 and 2693 Ma. Given the zircon U-Pb ID-TIMS age of 2698.0 ± 0.9 Ma for the tonalite megablock within the breccia, a permissible age range for brecciation and mineralization is 2698.9–2693 Ma, which is consistent with a minimal time gap between the crystallization of the tonalite and the

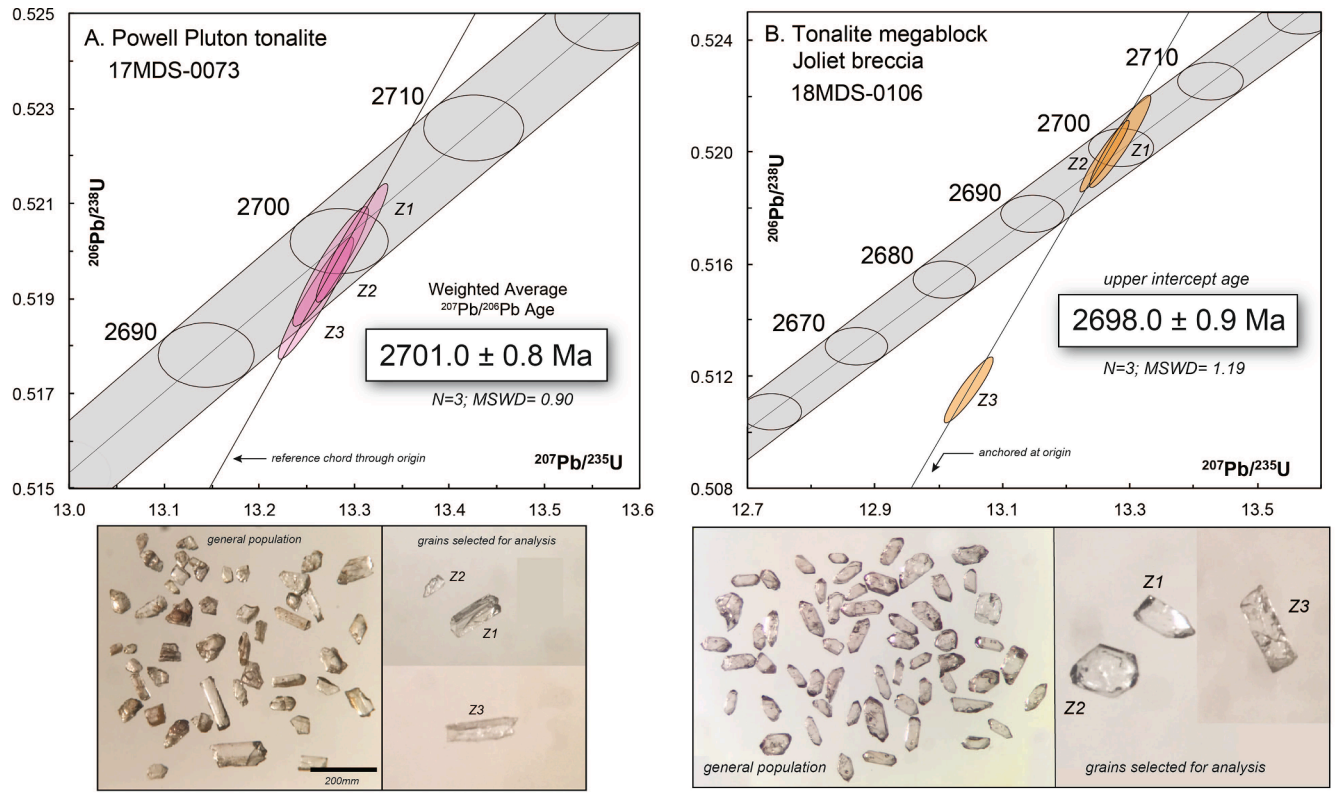

Fig. 6. Zircon grain images and Concordia diagrams for ID-TIMS U-Pb analyses from selected tonalite bodies in the eastern Powell Block.

mineralization. A number of grains displayed thin rims identified in high-contrast BSE, which were analyzed with a smaller spot size and yielded $^{207}Pb/^{206}Pb$ spot dates ranging from ~2700–2515 Ma, with small apparent sub-populations at ~2665 and 2620 Ma, indicating minor monazite growth or recrystallization during these time periods.

4.5.3. Vein mineralization

Cross-cutting, sulfide-bearing veins have sharp margins, typically range in width from 0.5 to 2 cm, are boudinaged, and strike 055° and dip 86°. The veins are zoned and have an outer margin of chlorite ± medium-coarse grained tabular quartz crystals and an interior of fine-grained, grey subhedral-euhedral granular quartz, acicular chlorite and sulfides. Sulfides are massive, vuggy and porous, consisting of subhedral to euhedral pyrite 0.5–1 mm diameter and anhedral interstitial chalcopyrite, rimmed by red iron-oxide. Locally, thin ~1 mm diameter, boudinaged calcite veins cross-cut the sulfide veins.

4.5.4. Metal zonation

Mapping indicates that the sulfide minerals are spatially restricted to the central area of the chloritized mafic dominated domain between tonalite blocks to the north and the felsic-transitional domains to the south. To determine spatial variations in metal tenor and association, 54 samples were collected along N-S and E-W oriented lines that cross the Joliet Breccia (Fig. 7).

There is considerable scatter in the absolute metal content of samples, reflecting the nugget-like distribution of sulfides within the breccia. Average values for select trace and major elements within each lithology are presented in Table 2. The Joliet Breccia is gold-poor, the highest value being 0.039 ppm Au, with an average value of 0.009 ppm Au. However, the breccia is relatively enriched in Ag, Bi, Te, Cu, Zn, As, Sn and W relative to the host rocks. In addition, the average value of Mo is slightly enriched in the felsic dominated domain, Joliet Breccia tonalite and Quemont feeder dike relative to more mafic lithologies.

4.6. Hydrothermal alteration

Four alteration types are recognized based on distinctive mineral associations. Mineral association refers to alteration or metamorphic minerals that occur together, are characteristic of a given alteration type, but may not be in equilibrium or have formed at the same time (Einaudi et al., 2003). All lithologies have experienced subgreenschist facies metamorphism, and virtually all samples contain some albite, quartz, chlorite ± sericite.

4.6.1. Quartz-albite alteration

Quartz-albite alteration is restricted to quartz-feldspar porphyritic rhyolite clasts derived from the Quemont feeder dike within the mafic dominated domain; it does not cross-cut the breccia. This alteration imparts a bleached, white appearance to clasts, in contrast to the yellow-beige or green alteration that characterizes sericite and chlorite alteration respectively (Fig. 10A). This alteration is fracture controlled and is manifest by a patchy to mesh textured distribution, with internal, angular areas between fractures of darker least altered rock. The contact between the darker least altered core areas and adjacent quartz-albite altered Quemont feeder dike is gradational over 0.5–1 mm and is cross-cut by fractures filled with vuggy quartz and sulfides that separate *in-situ* brecciated, jig-saw fit clasts (Fig. 10B). The leucocratic, quartz-albite altered zones are fine-grained and consist of randomly oriented albite (~70–130 μm) and quartz (~120–250 μm) with trace chlorite (Fig. 10C). The darker, least altered areas between fractures preserve a fine-grained mosaic of anhedral rounded quartz and albite (~30–60 μm) as sector recrystallized spherulites, and anhedral, interstitial chlorite (~30%).

4.6.2. Sericite alteration

The sericite alteration occurs in the coherent Quemont feeder dike and felsic clasts in the Joliet Breccia. It is characterized by a distinct,

Table 1
Zircon U-Pb isotopic data for eastern Powell block tonalite samples.

Fraction	Description	U (ppm)	Pb^T (pg)	Pb_C (pg)	Th/U	$^{206}Pb/^{204}Pb$	$^{206}Pb/^{238}U$	± 2 s	$^{207}Pb/^{235}U$	± 2 s	$^{207}Pb/^{206}Pb$	± 2 s	$^{206}Pb/^{238}U$	± 2 s	Ages (Ma) $^{207}Pb/^{235}U$	± 2 s	Ages (Ma) $^{207}Pb/^{206}Pb$	± 2 s	Disc. (%)
17MDS-0073; Powell pluton tonalite																			
Z1	1 clr, cls, lrg, el & irreg	856	2044.6	0.33	2.147	262,028	0.520177	0.001005	13.29681	0.03087	0.185394	0.000149	2699.9	4.3	2701.0	2.2	2701.7	1.3	0.1
Z2	1 clr, cls, sm shard	232	145.78	1.48	0.799	5240	0.519688	0.001014	13.27452	0.03246	0.185257	0.000179	2697.9	4.3	2699.4	2.3	2700.5	1.6	0.1
Z3	1 clr, cls, lrg, el & irreg	233	183.43	0.93	2.102	8342	0.519029	0.001035	13.25888	0.03218	0.185274	0.000160	2695.1	4.4	2698.3	2.3	2700.7	1.4	0.3
18MDS-0106; Joliet Breccia tonalite																			
Z1	1 clr, cls, sm brkn el fct pr	61	35.43	0.46	0.433	4417	0.520416	0.001347	13.28258	0.03983	0.185110	0.000198	2700.9	5.7	2699.9	2.8	2699.2	1.8	−0.1
Z2	1 clr, cls, stubby fct pr	199	117.07	0.19	0.482	34,863	0.519888	0.001032	13.25761	0.03152	0.184950	0.000145	2698.7	4.4	2698.2	2.2	2697.8	1.3	0.0
Z3	1 clr, cls, brkn el pr, sq, crk	137	164.48	1.97	0.633	4588	0.511588	0.000968	13.04357	0.03160	0.184916	0.000186	2663.4	4.1	2682.8	2.3	2697.5	1.7	1.5

Notes:
All analyzed fractions represent best optical quality (crack-, inclusion-, core-free), fresh (least altered) grains of zircon. Zircons were chemically abraded.
Abbreviations: Z – zircon; clr – clear; cls – colourless; crk – cracked; el – elongate; pr – prism/prismatic; fct – faceted; brkn – broken; sq – square cross-section; lrg – larger; sm – smaller; irr – irregular.
Pb^T is total amount (in picograms) of Pb.
Pb_C is total measured common Pb (in picograms) assuming the isotopic composition of laboratory blank: 206/204–18.221; 207/204–15.612; 208/204–39.360 (errors of 2%).
Pb/U atomic ratios are corrected for spike, fractionation, blank, and, where necessary, initial common Pb; 206Pb/204Pb is corrected for spike and fractionation.
Th/U is model value calculated from radiogenic 208Pb/206Pb ratio and 207Pb/206Pb age, assuming concordance.
Disc. (%) - per cent discordance for the given 207Pb/206Pb age.
Uranium decay constants are from Jaffey et al. (1971).

yellow-beige colouration and is subdivided into two alteration styles: 1) fracture controlled, and 2) pervasive. Fracture controlled sericitization occurs as haloes, on average 4–8 cm wide, that envelope conjugate fracture sets within the Quemont feeder dike (Fig. 10D). The fractures are also observed within large blocks of quartz-porphyritic rhyolite within the breccia. Pervasive sericite alteration is characteristic of the felsic dominated domain, where smaller clasts of Quemont feeder dike are pervasively sericitized (Fig. 4D). However, larger Quemont feeder dike clasts (≥0.5 m) within all domains of the breccia have preserved least altered interiors and a gradational boundary to a symmetrical, strongly sericitized clast margin (Fig. 10E-F). Sericite alteration consists of muscovite (20–30%) and quartz (70–75%) and minor chlorite (1–10%). It is associated with complete destruction of feldspar, wherein albite is pseudomorphed by fine-grained sericite ± chlorite.

4.6.3. Chlorite alteration

Chlorite alteration is limited to the mafic dominated and transitional domains of the Joliet Breccia. It is manifest by green alteration rims that mantle dominantly mafic clasts (Figs. 10E and 10G), in addition to previously quartz-albite or sericite altered felsic clasts within the mafic dominated domain (Fig. 10H). Clasts <40 cm in size are pervasively chloritized. Chlorite alteration obscures clast textures, and it is difficult in the field to distinguish chloritized clasts from chlorite cement (Fig. 10G). However, chlorite cement is restricted to vugs and tends to be coarser grained than chlorite within the altered margins of clasts (Fig. 10H). Chlorite alteration consists of fine-grained, distinctly green, Fe-rich chlorite, 60–70%, quartz, 5–10%, sericite 10–20%, albite 5–10% ± calcite ± chalcopyrite ± pyrite.

4.6.4. Spotted-textured alteration

The spotted-textured alteration manifests as ovoid, leucocratic "spots" 0.4–1 cm in diameter. Spotted-textured alteration is not uniformly distributed, and is limited to altered zones of clasts within the breccia and within sericite altered envelopes along conjugate fractures that occur up to 6 m from the outer Joliet Breccia contact. The spots are concentrated either in the interior (Fig. 10G) or margin (Fig. 10I) of chloritized mafic and sericite altered felsic clasts (Fig. 10J). However, spotted-textured alteration does not occur within the tonalite. The spots comprise fine-grained muscovite and quartz ± rutile ± albite, in a chloritized matrix (Fig. 10K) and have diffuse margins with the host rock; where numerous, the spots impinge and appear to merge (Fig. 10L). The spots within mafic clasts are typically larger and occur as protuberances (Fig. 10I) in comparison to those within felsic clasts, which do not stand out as readily (Fig. 10J). The spots are typically flattened parallel to the main E-W striking regional cleavage (Fig. 10K).

4.6.5. Alteration geochemistry

The alteration products are partly controlled by the primary bulk composition of the protolith, which is evident in the spatial distribution of the alteration types (Fig. 7). The higher Fe, Mg, Mn and Sc values of the mafic dominated domain favours chloritization, whereas higher K and Ba values of the felsic dominated domain, tonalite and fractured Quemont feeder dike favours sericitization. However, K, Ba, Fe, Sc and Mg are enriched in the felsic dominated and mafic dominated domains relative to the host Quemont feeder dike and Powell andesite (Table 2), indicating these elements were added by the hydrothermal fluid during alteration. In addition, average values for Ba, Fe, Sc and Mg are higher in the mafic and felsic dominated domains relative to the Joliet Breccia tonalite.

Compositional changes associated with each alteration type are calculated using Gresens (1967) mass change formula as modified by Babcock (1973), as outlined and graphically displayed in supplementary data file 5. Calculated compositional changes associated with each alteration type are consistent with the observed modal mineralogy. Sericite alteration is associated with significant gains in Si, Al, K, Rb, and Ba, and a decrease in Ca, Na, Mg, Mn, and Fe. Chlorite alteration is associated with

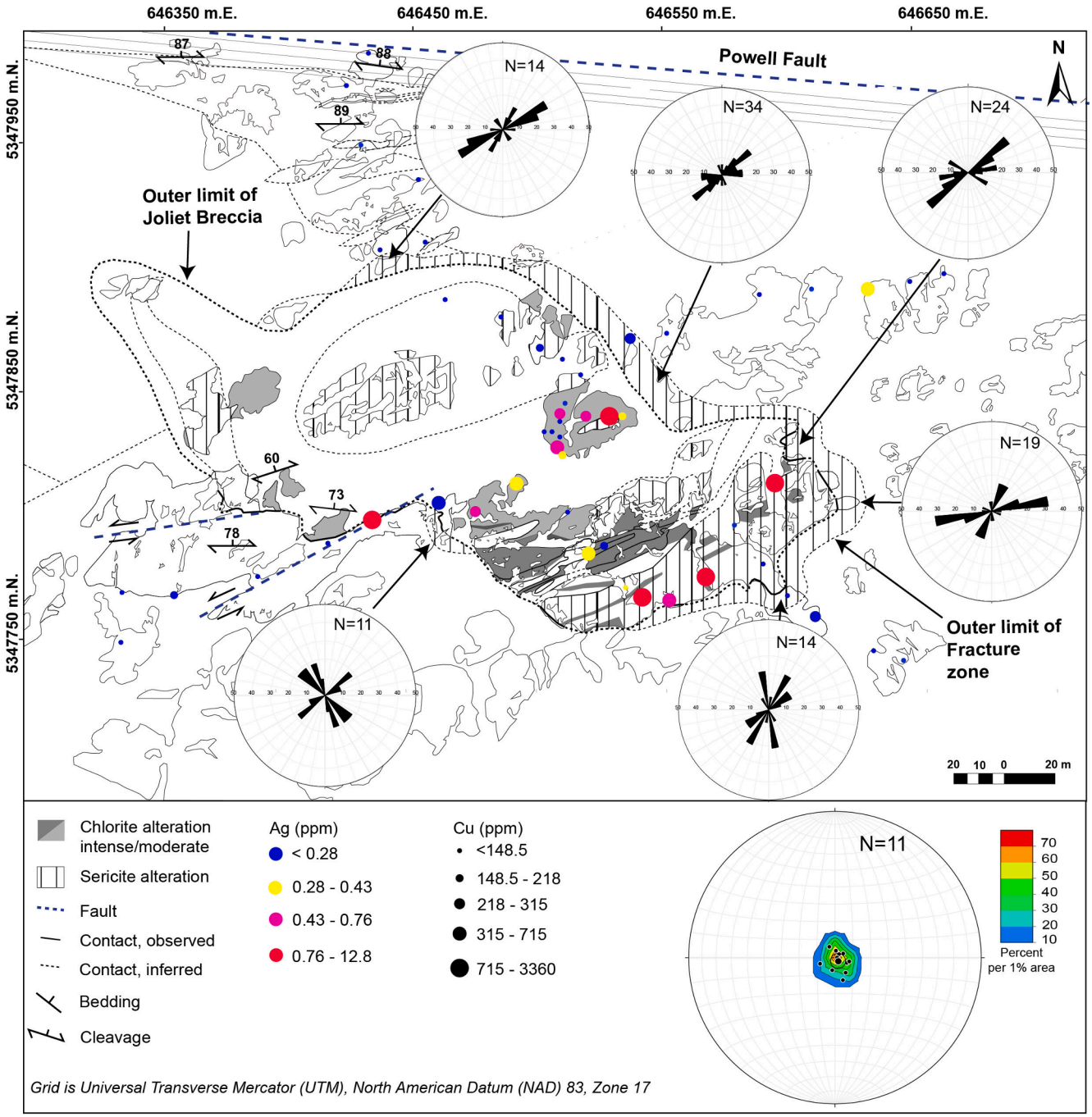

Fig. 7. Spatial distribution of Ag and Cu within the Joliet Breccia. The Ag and Cu concentrations are illustrated by colour and size of the symbols, respectively. Rose diagram insets show variation in orientations of conjugate fracture sets within the QFP dike surrounding the margin of the Joliet Breccia. Note, fractures are oriented both subparallel and radial to the outer contact of the breccia. Stereonet inset shows the mean vector for the line of intersection between conjugate fractures.

gains in Al, Fe, Sc and Ti and losses in Si, Na, K, Ca, Mg, Ba, Sr, Rb and Cr. In addition, the LREE are depleted relative to the HREE and HFS, which indicates potential mobility. Compositional gains and losses associated with spotted-textured alteration include major gains in Al, Rb, K, Ba, Fe (±Mg ± Mn) and Ti and losses in Na, (±Mg ± Mn), Ca and Sr. Losses in Na and Ca, associated with sericite and chlorite alteration reflect destruction of feldspar. Progressive alteration is demonstrated by increased values in the Ishikawa alteration index (AI: 100*[K2O + MgO]/[K2O + MgO + Na_2O + CaO]) and chlorite carbonate pyrite index (CCPI: 100*[MgO + FeO]/[MgO + FeO + Na2O + K2O]; Fig. 2, supplementary data file 5). The spotted-textured samples appear to have intermediate AI and CCPI values between least altered and chlorite altered samples (Fig. 2, supplementary data file 5).

5. Discussion

We first discuss potential mechanism(s) and timing for Joliet Breccia fragmentation and emplacement, and then discuss the relationship and timing of the Joliet Breccia alteration and mineralization relative to the formation of the breccia and the larger-scale metallogeny of the Rouyn-Noranda mining district. Based on the geologic attributes for the Joliet Breccia established in this study through mapping, geochemistry, and

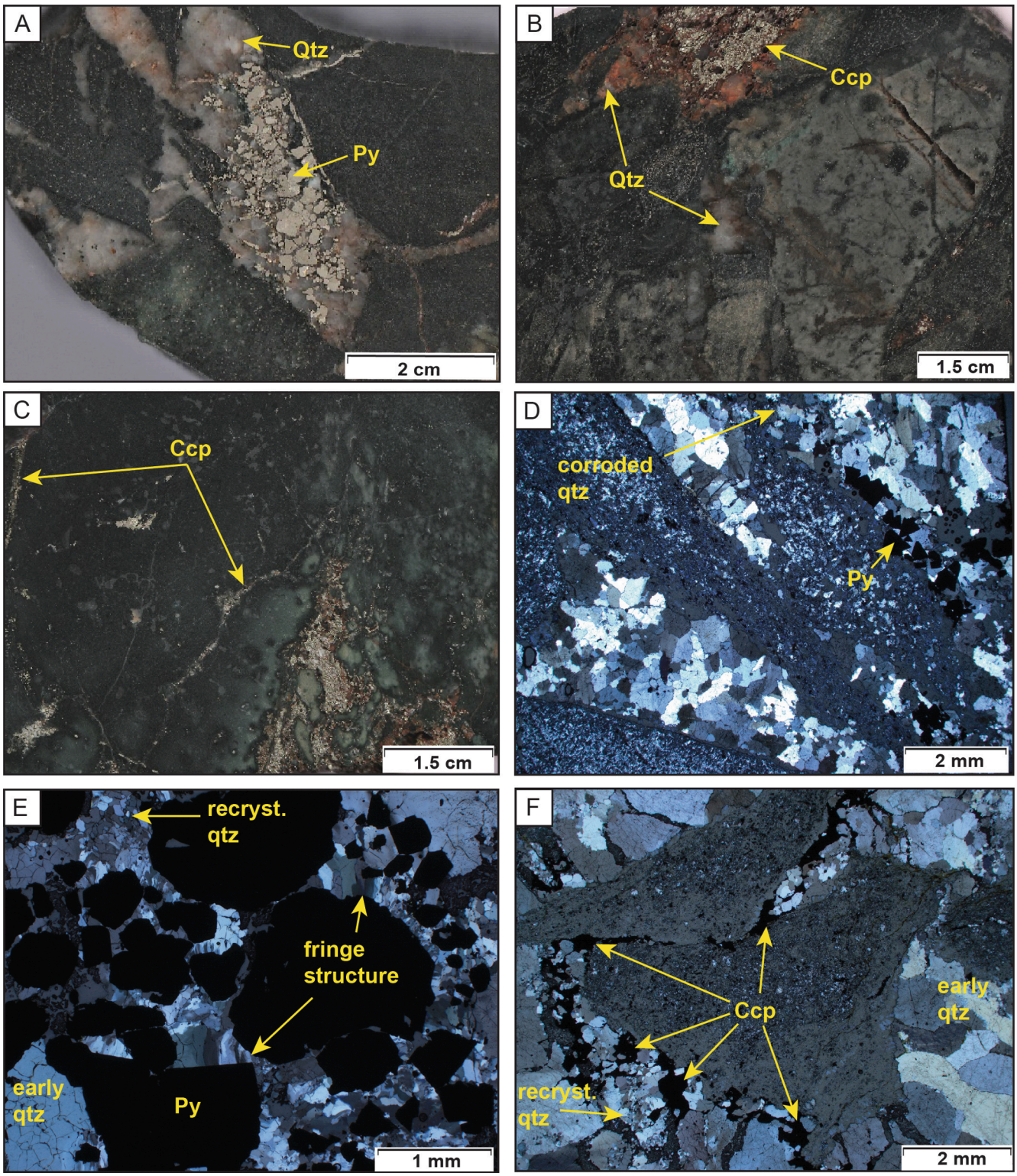

Fig. 8(A-F). A) Mafic dominated domain, showing angular chloritized mafic clasts with a white comb quartz cement, minor red staining, and coarse-grained euhedral pyrite (polished slab); B) Mafic dominated domain showing vug with strongly red stained quartz and internal massive chalcopyrite. Note the vug in the middle of the image, which lacks sulfides and appears pristine white (polished slab); C) Veinlets of chalcopyrite cross-cutting chloritized clasts and a vug associated with massive chalcopyrite, without quartz, and leucocratic alteration surrounding it (polished slab); D) Angular chloritized mafic clasts within mafic dominated domain. Vug cement in bottom of image shows white comb quartz, without sulfides, compare to vug in top right of image which contains euhedral pyrite along the margin of the clast (cross-polarized light); E) Fractured, white comb quartz cement with undulose extinction that is overgrown by a fine-grained polygonal quartz mosaic with recrystallized grain boundaries. Note, euhedral pyrite with fringe structures (cross-polarized light); F) Angular chloritized mafic clast surrounded by white comb-quartz. Note, fracturing and recrystallization of quartz along grain boundaries infilled by anhedral chalcopyrite and chlorite (cross-polarized light). (Ccp = chalcopyrite, Py = pyrite, Qtz = quartz, recryst. = recrystallized).

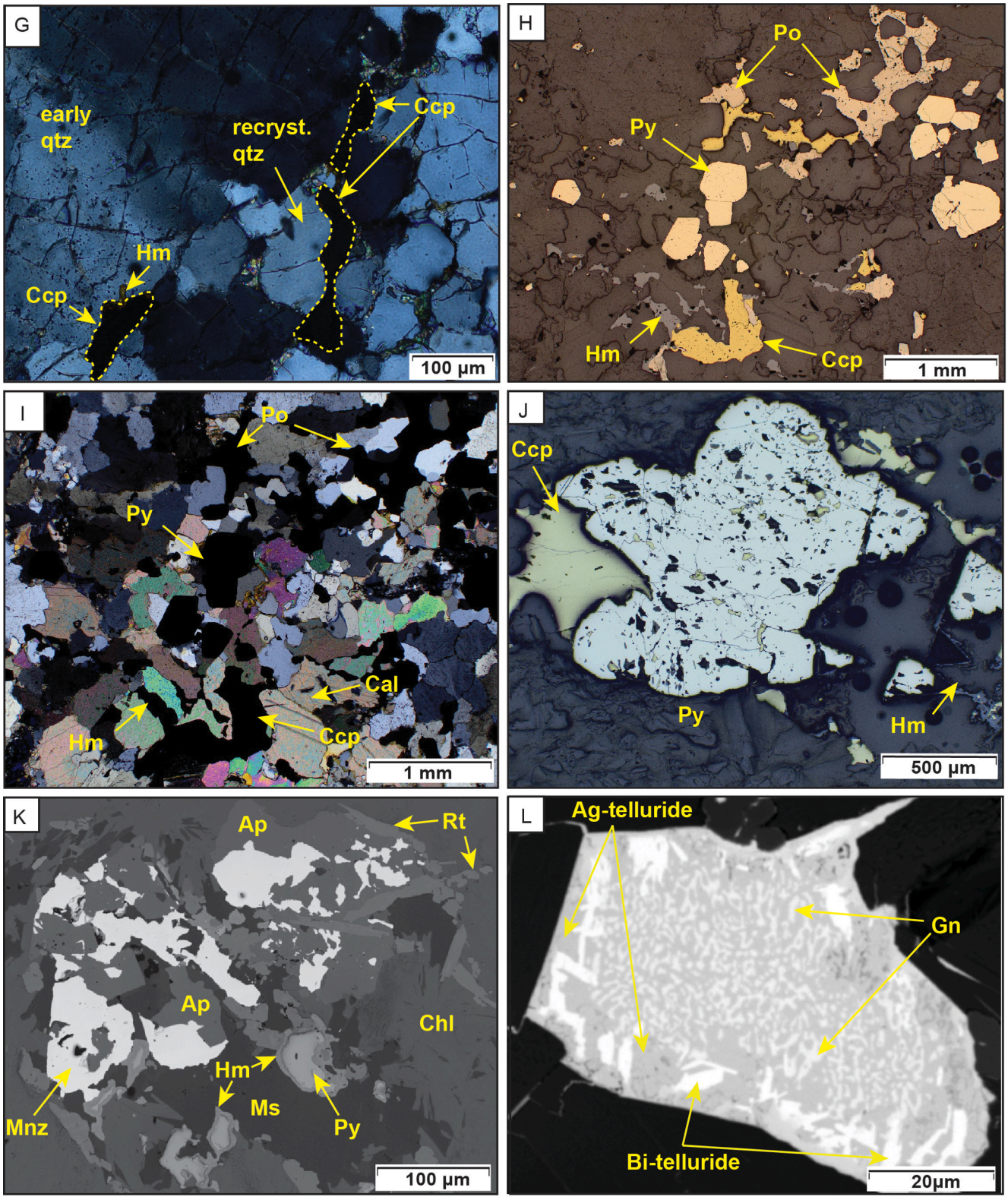

Fig. 8(G-K). G) Fracturing and undulose extinction within early comb quartz (top left), which is overgrown by a polygonal quartz mosaic (bottom right). Chalcopyrite occurs interstitial to polygonal quartz; H-I) Euhedral pyrite, anhedral intergrown pyrrhotite and chalcopyrite, in a quartz, calcite vug (H = reflected and I = cross-polarized light); J) Euhedral to subhedral pyrite and interstitial anhedral chalcopyrite, note numerous inclusions and cross-cutting veinlets of chalcopyrite within pyrite (cross-polarized light); K) Subhedral pyrite with hematite rims, intergrown with apatite, monazite, rutile, muscovite and chlorite within vug (back-scattered electron image, SEM); L) Ag-Bi telluride interstitial to chlorite within vug (back-scattered electron image, SEM). (Ap = apatite, Cal = calcite, Ccp = chalcopyrite, Gn = galena, Hm = hematite, Mnz = monazite, Po = pyrrhotite, Py = pyrite, Qtz = quartz, Rt = rutile).

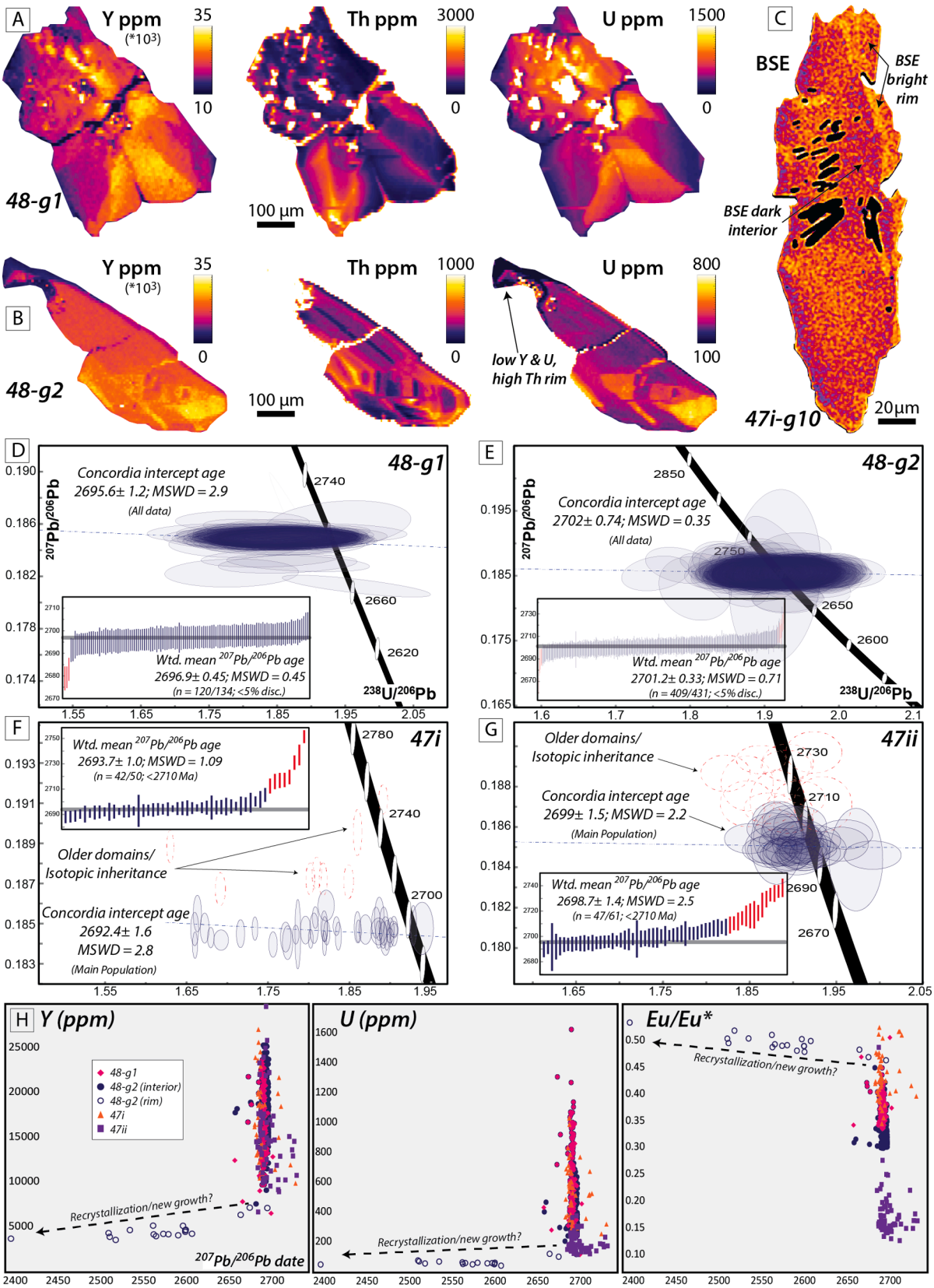

Fig. 9. LAICPMS monazite maps and data; A-B) Representative trace element concentration maps for monazite grains 1 and 2 from sample 48; C) Representative back scattered electron image of monazite from sample 47, showing a bright rim and a dark core; D-E) Concordia diagrams of all analyses for grains 1 and 2 from sample 48, with inset of weighted mean plots for <5% discordant analyses and 2σ outlier rejection; F-G) Concordia diagrams of all analyses for 16 grains from two subsamples of 47, with inset of weighted mean plots for <5% discordant analyses and 2σ outlier rejection; H) Plots of trace element concentration vs. $^{207}Pb/^{206}Pb$ spot date, showing similar range of concentrations for all grain interiors (except for 47ii), and depleted Y and U, and smaller Eu anomaly in thin rims of grains (interpreted as recrystallization or new growth).

Table 2
Average values for select trace and major elements by lithology.

				Mafic dominated domain[1]			Felsic dominated domain[1]			JB Tonalite[1]			Quemont feeder dyke[1]			Powell andesite[2]		
		L.L.O.D	U.L.O.D	Avg.	Std.	No.[3]	Avg.	Std.	No.[3]	Avg.	Std.	No.[3]	Avg.	Std.	No.[3]	Avg.	Std.	No.[3]
Ag	*ppm*	*0.01*	*100*	1.2	3.1	16	0.8	0.7	6	0.11	0.1	6	0.1	0.1	17	0.3	0.0	4
As	*ppm*	*0.2*	*10,000*	3.8	6.5	16	0.5	0.3	6	1.02	0.7	6	0.6	0.4	17	0.3	0.2	4
Bi	*ppm*	*0.01*	*10,000*	0.9	1.3	16	0.5	0.4	6	0.27	0.2	6	0.2	0.2	17	0.0	0.0	4
Te	*ppm*	*0.05*	*500*	0.1	0.2	16	0.3	0.2	6	0.06	0.0	6	0.1	0.1	17	0.0	0.0	4
Sb	*ppm*	*0.05*	*10,000*	0.1	0.1	16	0.1	0.0	6	0.07	0.0	6	0.1	0.0	17	0.1	0.1	4
Sn	*ppm*	*0.2*	*500*	8.9	3.9	16	5.4	3.1	6	2.80	1.4	6	3.5	2.8	17	2.2	0.9	4
W	*ppm*	*0.1*	*10,000*	2.1	1.4	16	3.6	6.1	6	0.32	0.2	6	0.6	0.5	17	1.1	0.0	4
Li	*ppm*	*0.2*	*10,000*	41.4	9.3	16	29.1	29.9	6	17.35	1.7	6	10.6	4.3	17	21.4	8.5	4
Cu	*ppm*	*0.2*	*10,000*	510	909	16	553	479	6	60.68	56.2	6	124	176	17	98.5	181	4
Zn	*ppm*	*2*	*10,000*	197	64.4	16	97.7	92.9	6	63.00	25.2	6	71.1	33.8	17	221	155	4
Pb	*ppm*	*0.5*	*10,000*	1.6	1.1	16	1.5	0.5	6	1.25	0.3	6	1.9	1.5	17	2.4	2.8	4
Mo	*ppm*	*0.05*	*10,000*	1.1	0.5	16	4.1	3.4	6	2.82	0.8	6	2.9	0.6	17	0.8	0.3	4
S	*%*	*0.01*	*10*	0.8	1.1	16	0.1	0.1	6	0.42	0.3	6	0.2	0.2	17	0.1	0.1	4
Fe	*%*	*0.01*	*50*	10.7	2.4	16	7.4	7.2	6	3.29	0.6	6	3.4	0.5	17	7.5	0.3	4
Sc	*ppm*	*0.1*	*10,000*	27.9	5.8	16	16.7	7.4	6	9.63	1.9	6	12.3	1.2	17	25.8	4.5	4
Mg	*%*	*0.01*	*50*	2.4	0.6	16	1.7	2.0	6	0.54	0.1	6	0.4	0.2	17	3.9	0.9	4
Mn	*ppm*	*5*	*100,000*	1512	414	16	550	490	6	537	36.8	6	686	301	17	0.2	0.1	4
K	*%*	*0.01*	*10*	0.8	0.5	16	0.5	0.5	6	0.52	0.3	6	0.2	0.2	17	0.2	0.1	4
Rb	*ppm*	*0.1*	*10,000*	9.3	6.8	16	10.6	10.5	6	12.20	7.8	6	4.6	4.5	17	5.6	3.6	4
Sr	*ppm*	*0.2*	*10,000*	50.1	48.3	16	17.7	9.0	6	93.50	45.1	6	43.7	13.8	17	60.2	20.5	4
Ba	*ppm*	*10*	*10,000*	309	251	16	162	150	6	137	73.1	6	52.9	51.0	17	96.2	1.6	4
P	*ppm*	*10*	*10,000*	628	180	16	388	435	6	413	116.9	6	150	18.4	17	990	429	4
Na	*%*	*0.01*	*10*	1.2	1.0	16	1.6	1.5	6	2.74	0.4	6	3.7	0.3	17	3.5	0.4	4
Ca	*%*	*0.01*	*50*	1.0	1.0	16	0.1	0.1	6	1.26	0.6	6	0.6	0.4	17	2.0	1.2	4

[4]Fe is corrected to sulfide free values, assuming all sulfides are present as pyrite using the equation: $Fe_{sulfide\ free} = Fe\ wt\%_{measured} - (46.55*S\ wt\%_{measured})/53.45$.
[1] Data for mafic dominated domain, felsic dominated domain, Joliet tonalite and Quemont feeder dike from 4 acid digestion (ME-MS61).
[2] Data for Powell andesite from whole rock data (CCPKG01).
[3] Values below the detection were assigned half of the value of the detection limit.

geochronology, any model attempting to explain Joliet Breccia fragmentation and emplacement processes must satisfy the following constraints:

1. The gradational contacts between different breccia domains within the breccia, and between the Joliet Breccia and the immediate host rocks;
2. Fracturing and *in situ* brecciation of the host Quemont feeder dike in proximity to the Joliet Breccia;
3. Hydrothermal cement of the Joliet Breccia and surrounding *in situ* brecciated host rocks with a total absence of a fine-grained, clastic, ash-sized matrix;
4. Poor size sorting and absence of bedding, with breccia domains defined by dominant clast composition, which reflects the composition of adjacent host rocks;
5. Abundance of lithic clasts with an angular blocky to tabular morphology, including blocks of the upper marker unit;
6. Brecciation of a tonalitic intrusion and tonalite blocks in the Joliet Breccia;
7. A U-Pb zircon age of 2698.0 ± 0.9 Ma for the brecciated tonalite intrusion, and four hydrothermal monazite ages (2693.7 ± 1.0/8.9 Ma; 2696.9 ± 0.45/8.9 Ma; 2698.7 ± 1.4/8.9 Ma; 2701.2 ± 0.33/8.9 Ma; 2 s/2s_{sys}), which indicates that the brecciation and hydrothermal filling of vugs at the Joliet Breccia is 0.3–8.7 Ma younger than the 2702 ± 0.8 Ma synvolcanic Quemont feeder dike host and surrounding volcanic rocks;
8. Its formation prior to regional deformation, since the Joliet Breccia, host rocks, alteration and mineralization are overprinted by the regional ca. <2669–>2639 Ma age cleavage.

5.1. Previously proposed model for the Joliet Breccia

Wilson (1941), Lichtblau and Dimroth (1980), Lichtblau (1989), Dimroth and Rocheleau (1979) and De Rosen Spence (1976) attributed the formation of the Joliet Breccia to an explosive, subaqueous phreatic eruption and they invoked phreatic explosion breccia craters at Yellowstone (Muffler et al., 1971) as a subaerial analogue. The interpreted driving mechanism for brecciation was the heat of a cooling Quemont feeder dike. Dimroth and Rocheleau (1979) and Lichtblau (1989) interpreted the internal clast domains identified herein to be conformable depositional units deposited on the seafloor, which they subdivided into a lower "cycle 1", and an upper "cycle 2". "Cycle 1" was interpreted as an interbedded sequence of "mixed breccia" containing a few mafic blocks and "brecciated rhyolite", which corresponds to the transitional and felsic dominated domains of this study, respectively. They described "cycle 2", or the mafic dominated domain herein, as a mafic and mixed breccia, consisting of a chaotic assortment of angular Quemont feeder dike blocks and Powell andesite blocks, with an increase in proportion of andesite blocks towards the top of the sequence. They viewed the WSW striking breccia domains and the E-W trending long axis of the blocks within the breccia to define bedding and to mark the paleohorizontal. The western and eastern margins of the Joliet Breccia were described as the steeply dipping inner crater walls (Lichtblau, 1989). To justify the current geometry of the Joliet Breccia and host rocks, Lichtblau (1989) envisaged that originally, the Quemont feeder dike dipped shallowly towards the north and the base or deeper part of the explosion crater to lie to the south within the host Quemont feeder dike. Tonalite within the Joliet Breccia was interpreted as younger dikes cross-cutting the breccia (Lichtblau, 1989) and thus post-dating and unrelated to the brecciation and mineralization events.

Lichtblau (1989) proposed that the upper marker unit of the Powell formation is the distal, basin-ward equivalent of "cycle 2", thus correlating the Joliet Breccia with the host volcanic strata ca. 2704–2701 Ma (McNicoll et al., 2014). However, blocks of the upper marker unit within the Joliet Breccia, and a new U-Pb zircon age of 2698.0 ± 0.9 Ma for a tonalite block within the breccia indicate that the Joliet Breccia is 0.3–8.7 Ma younger than the Quemont feeder dike, Powell formation

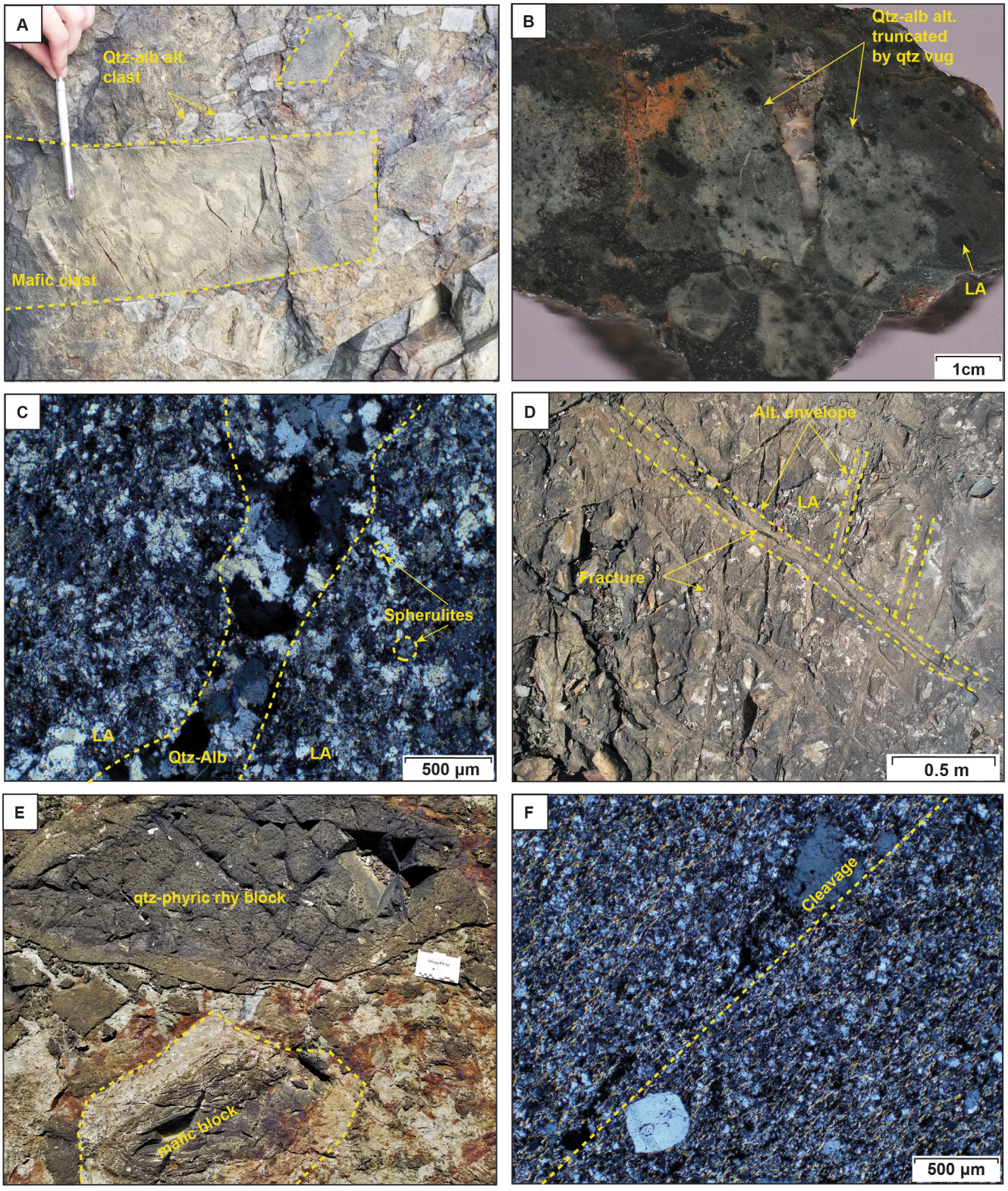

Fig. 10(A–F. A) Quartz-albite altered clasts within the mafic dominated domain (field photograph); B) Quartz-albite alteration within a quartz-feldspar porphyritic rhyolite clast within the mafic dominated domain, note darker areas (least altered cores). Alteration truncated by quartz-vug. (polished slab); C) Diffuse, gradational contact between quartz-albite alteration and least altered quartz-feldspar porphyritic rhyolite clast. Note, change in quartz grain size, and destruction of spherulitic texture (cross-polarized light); D) Sericite alteration envelope surrounding fractures within the Quemont feeder dike; E) Chlorite and sericite alteration rims mantling clasts within the mafic dominated domain. Yellow, sericite rim around quartz porphyritic clasts, and green chlorite rims around mafic clasts (field photograph); F) Sericite alteration. Note well-developed foliation defined by muscovite (cross-polarized light).(Alt. = alteration, LA = least altered, Qtz-Alb = quartz-albite).

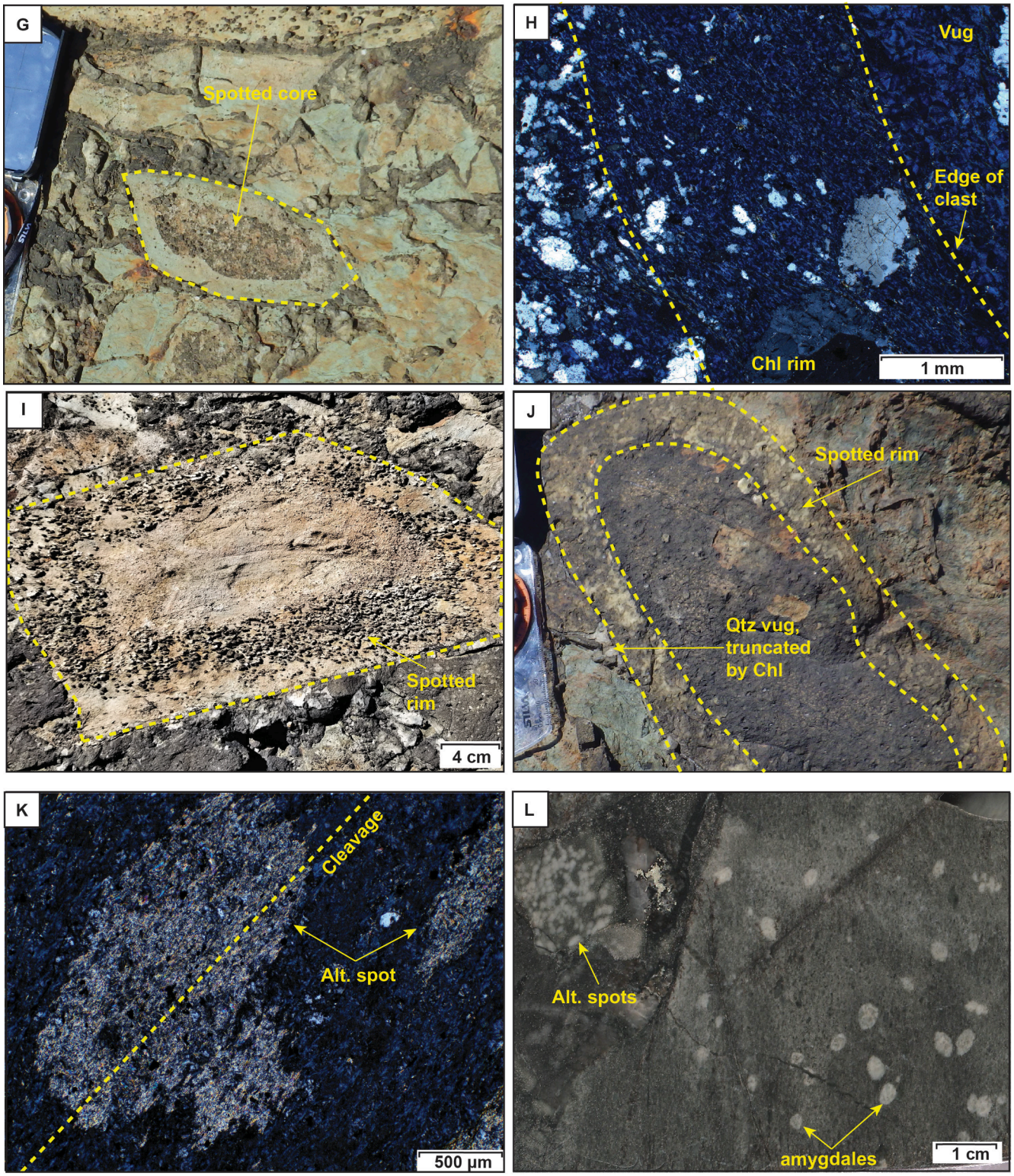

Fig. 10(G–L. G) Intense chlorite alteration of mafic clast rims and weakly chloritized and spotted-textured core of mafic clasts, within mafic dominated domain (field photograph); H) Gradational contact with fine-grained chlorite alteration rim around quartz feldspar porphyritic rhyolite clast. Note, coarse grained chlorite in vug (cross-polarized light); I) Spotted-textured alteration rim of a weakly chloritized mafic clast (field photograph); J) Spotted-textured alteration rim around quartz feldspar porphyritic rhyolite clast (field photograph); K) Alteration spot in chloritized mafic clast overprinted by regional cleavage. L) Grey alteration spots with diffuse margins within felsic clast, compared to amygdales in adjacent clast with sharp margins (polished slab). (Alt. = alteration, Chl = chlorite).

and Quemont VMS deposit and is time equivalent to the youngest units of the Blake River Group (ca. <2699.5–2697 Ma; McNicoll et al., 2014). Furthermore, the contacts between inferred beds, now interpreted as clast domains, are gradational as is the contact between the Joliet Breccia and host Quemont feeder dike, plus the complete lack of sedimentary features and blocks of younger tonalite indicate the Joliet Breccia formed in the subsurface and may or may not have breached the seafloor.

The occurrence of well bedded clasts of Powell tuff, massive amygdaloidal and pillowed andesite, and lapilli-tuff of the upper marker unit and massive aphanitic and quartz-microporphyritic rhyolite implies some vertical transport and or downward settling. The lack of a chilled margin and the presence of clasts of tonalite within the Joliet Breccia indicate that the tonalite was intruded prior to the formation of the mafic dominated domain of the Joliet Breccia.

5.2. Possible fragmentation processes for the Joliet Breccia

The abundance and anomalous size of lithic clasts with an anisometric clast size distribution within the Joliet Breccia, is consistent with sudden steam generation within the host rock and spalling, with high energy due to voluminous explosive vapor expansion (Fisher and Schmincke, 1984; Jébrak, 1997). Possible explosive fragmentation processes consistent with features of the Joliet Breccia include hydrovolcanic and magmatic-hydrothermal processes. Tectonic implosion may also produce similar features (Mitcham, 1974; Sibson, 1986; Jébrak, 1997). All three fragmentation mechanisms can result in monomictic to polymictic breccias, gradational contacts with host rocks and an angular clast morphology (Table 3) depending on the nature of the host-rocks, intensity of the brecciation event and confining pressure, which dictates the amount of movement and particle attrition of the resultant breccia (Fisher and Schmincke, 1984). The angularity of clasts in the Joliet Breccia and lack of a clastic matrix indicates virtually no particle attrition, and the linear, dike parallel orientation of the clast domains rather than a symmetrical or annular distribution implies dominantly local derivation of clasts from the immediate host rocks, and minimal transport or fluidisation (Reynolds, 1954).

Explosive hydrovolcanic processes operate at or near surface, involve an external fluid source (meteoric or seawater), and are subdivided into phreatic and phreatomagmatic, based on evidence for indirect or direct contact with magma, respectively. A phreatic brecciation mechanism is caused by flashing of an external fluid to steam as a result of contact with hot rocks that were conductively heated by magma (Browne and Lawless, 2001). In contrast, a phreatomagmatic brecciation mechanism requires evidence for direct interaction between an external fluid and magma, as indicated by a juvenile component to the breccia that is usually present in the matrix (Lorenz, 1973; Fisher and Schmincke, 1984; White and Ross, 2011).

Tectonic-hydrothermal breccias form near surface in the upper 10–15 km of crust, associated with active faults and unlike hydrovolcanic breccias do not require a direct input of magmatically derived mass or energy (Sibson, 1986; Jébrak, 1997; Woodcock and Mort, 2008). Fault associated breccias are formed by a variety of physical processes, however, this discussion is limited to fluid assisted brecciation, also known as implosion brecciation (Sibson, 1986), as it is the only viable tectonic-hydrothermal process that may produce the features observed in the Joliet Breccia. Implosion brecciation is triggered by a decrease in pressure at releasing bends or dilational jogs along fault surfaces and at intersections between two growing faults (Mitcham, 1974; Sibson, 1986; Jébrak, 1997).

Magmatic-hydrothermal brecciation requires the separation of a volatile phase from an associated crystallizing magma as a result of second boiling and subsequent decompression, vaporization and rapid volatile expansion to trigger an explosive event (Sillitoe, 2010), as opposed to the externally derived fluid involved in hydrovolcanic processes (Fisher and Schmincke, 1984; Sillitoe, 2010). These systems

Table 3
Distinguishing characteristics of breccias.

Category	Other names	Distinguishing textures	Diameter (m)	Geometry	Clast morphology	Clast size distribution	Matrix	Related intrusive rocks	Alteration	Examples	Ref.
Phreatic	Hydrothermal explosion/ eruption	Jig-saw fit, exfoliated fragments, sinter fragments (hydrothermally altered clasts)	up to ~500	pipes, but commonly irregular or pebble dikes	typically polymictic, angular-rounded	anisometric	rock flour (<50%) and/or hydrothermal cement	yes	widespread silicification common, argillic, advanced argillic, sericite, chlorite	Equity Silver, B.C. Canada; Round Mountain, Nevada;	Sillitoe (1985)
Implosion	Fluid-assisted breccia Hydrothermal breccia	Jig-saw fit	~50	steep tabular bodies, or pipes, occurs along dilational jogs in active structures	typically monomictic, angular	typically isometric	hydrothermal cement	no	variable	Martha Mine, New Zealand; Cinola deposit, B.C. Canada	Mitcham (1974), Sibson (1986), Jébrak (1997)
Magmatic-hydrothermal	Intrusion-related/Porphyry	Jig-saw fit, sheeted contacts, shingle breccia, exfoliated fragments	50–300, locally >1000	single or multiple pipes	typically monomictic, angular-rounded	anisometric	rock flour (<30–50%) and/ or hydrothermal cement	yes	biotite and/or k-silicate common, sericite, chlorite, quartz-topaz, tourmaline	Galore Creek, B.C. Canada; Red Mountain, Arizona	Sillitoe and Sawkins, 1971, Sillitoe (1985), Sillitoe (2010)

are common in young arcs and active settings (e.g., El Teniente, central Chile; Camus, 1975), and their recognition in Archean greenstone belts is relatively rare (e.g., Côté Gold, Katz et al., 2017). The breccias are associated with plutons or stocks, and can host small volumes of fine-grained porphyritic intrusions in the form of dikes, small bodies, angular fragments and/or irregular, partly disaggregated masses, which indicates a temporal, spatial and likely genetic relationship to the breccia (Sillitoe, 1985).

The Joliet Breccia is spatially associated with a major synvolcanic structure now occupied by the Quemont feeder dike. The sharp, intrusive contact of the northernmost Quemont dike with the host volcanic strata is not sheared and evidence for lateral movement along the Quemont feeder dike is lacking. In addition, the anisometric clast size distribution and polymictic nature of the clasts in the Joliet Breccia and spatial association with intrusive rocks is atypical of implosion breccias (Table 3). Subsea-floor phreatic, magmatic-hydrothermal and phreatomagmatic explosive activity remain as the most likely processes, but the latter is negated by the lack of a juvenile component as clasts or matrix in the Joliet Breccia. The main distinguishing feature that separates phreatic breccias from magmatic-hydrothermal breccias is the widespread silicification that may be associated with the former, both as a pervasive replacement of clasts and as hydrothermal cement, with a close relationship between silicification and brecciation as an episodic self-sealing-rupture mechanism (Gibson et al., 1983; Sillitoe, 1985; Gibson, 2005). The spatial association with a tonalitic intrusion suggests the input of magmatic heat, ± volatiles ± metals to the system, likely at depth and generated from the same source as the Flavrian-Powell Intrusive Complex due to their similar mineralogy and geochemistry. This would be conducive to either a phreatic or magmatic-hydrothermal explosive event, depending on the indirect or direct role of magmatic volatiles, respectively. The radial and concentric orientations of the fractures surrounding the Joliet Breccia are suggestive of a uniaxial stress regime above a cylindrical stock typical of magmatic-hydrothermal environments (Koide and Bhattacharji, 1975; Tosdal and Richards, 2001). This suggests that a magmatic-hydrothermal mechanism is the most likely brecciation process for the Joliet Breccia (Sillitoe and Sawkins, 1971).

A minimum of two brecciation events within the Joliet Breccia are indicated by the presence of blocks of *in situ* brecciated felsic dominated domain within the mafic dominated domain. In addition, the lack of the spotted-textured alteration within the tonalite, implies that it had not experienced the same degree of alteration as the pervasively sericitized and spotted felsic dominated domain. This, combined with the brecciated contact of the tonalite in the mafic dominated domain, and presence of cross-cutting sericitized fractures within the tonalite, suggests it was emplaced after the formation of the felsic dominated domain and prior to the formation of the mafic dominated domain (Fig. 11). The Joliet Breccia is broadly discordant based on cross-cutting relationships. Assuming formation driven by uniaxial extensional stresses, the long axis represented by the intersection of surrounding conjugate fractures would be parallel to the orientation of the breccia body (Koide and Bhattacharji, 1975; Tosdal and Richards, 2001), implying a possible sub-vertical geometry in this case (Fig. 3). These fractures were likely purely tensile as indicated locally by fibrous quartz growing perpendicular to the fracture margin.

5.3. Distinguishing subsurface vs. surface breccias in the ancient rock record

Distinguishing between surface and subsurface breccias is essential for stratigraphic reconstruction and exploration, particularly in VMS districts where coarse breccias, particularly those dominated by felsic clasts, commonly define favourable stratigraphic intervals associated with VMS deposits (Franklin et al., 2005). Using the Joliet Breccia as an example, features essential to recognizing subsurface breccias in ancient deformed terranes include:

1. Discordant contact with host rocks. This requires knowledge of the stratigraphy and structure, i.e., the development of the volcanic succession and deformation history;
2. Gradational contact with host rocks. Subsurface breccias are often surrounded by a gradational damage zone, associated with fracturing and *in situ* brecciation of host rocks;
3. A vuggy, open space matrix, which is characteristic of many subsurface breccias and is atypical of conformable volcanic breccias. In subsurface breccias the vuggy open-space matrix is typically infilled with hydrothermal minerals deposited syn or post brecciation. Some subsurface breccias are associated with a clastic, ash-sized matrix that may be massive and homogeneous or display fine lamination that developed during emplacement (Fisher and Schmincke, 1984; Sawkins, 1990). In the latter, careful mapping to define contact relationships and to establish discordance are required;
4. Inter-breccia intrusions, and angular lithic blocks of intrusive rocks within the breccia;
5. Timing of the breccia and host rocks. This can be relative, based on cross-cutting relationships and relationship to tectonic fabrics (deformation history) or absolute, based on dating of blocks, matrix and host rocks.

5.4. Mineralization and associated hydrothermal alteration

Chalcopyrite, pyrite, and pyrrhotite are dominantly in the matrix of the breccia and, to a lesser extent, in veins that cut the breccia indicating that mineralization occurred syn- to post-brecciation. Textural relationships such as the fractured, recrystallized and red staining of white coarse-grained comb quartz where associated with sulfides, and the observation that white comb quartz and sulfides occur together and separately within the breccia cement, suggest that the quartz formed early relative to the sulfides. The euhedral habit of the pyrite compared to the interstitial anhedral habit of chalcopyrite and pyrrhotite and the presence of corroded pyrite grains with cross-cutting chalcopyrite micro veinlets is likely related to post-mineralization deformation, wherein pyrrhotite and chalcopyrite are preferentially remobilized relative to pyrite (Gilligan and Marshall, 1987). This is supported by the presence of chalcopyrite interstitial to recrystallized quartz. Calcite veins cross-cutting Joliet Breccia clasts and matrix cement, and locally infilling remaining void space within matrix vugs represents the youngest event. The observed paragenesis of the hydrothermal cement at the Joliet Breccia is consistent with the expected paragenesis for magmatic-hydrothermal breccias, which typically consists of early tourmaline (where present), followed by quartz, then sulfides, and finally late carbonate minerals (Sillitoe and Sawkins, 1971; Sillitoe, 1985). The red staining results from oxidation of sulfides at surface.

The Joliet Breccia alteration consists of the low-temperature (<300 °C) mineral associations of chlorite, sericite and carbonate minerals (Sillitoe, 2010) consistent with many magmatic-hydrothermal breccias that have exclusively sericitic and/or chloritic alteration down to their roots (Table 3; Sillitoe and Sawkins, 1971), and notably is also typical of VMS deposits. The alteration types are divisible into pre-, syn-, and post- breccia events, based on textural and spatial relationships. The quartz-albite alteration is the earliest alteration as it is confined to select clasts within the Joliet Breccia where it is truncated by white comb quartz-lined fracture controlled vugs. The sericite and chlorite alteration occurred *syn*-brecciation as indicated by their symmetrical, concentric pattern around clasts. However, chlorite alteration is later as evidenced by the presence of pervasively sericitized blocks of the felsic dominated domain, overprinted by chlorite alteration within the chloritized mafic dominated domain (Fig. 4I). In addition, the gradual increase in matrix chlorite towards the transitional domain and mafic dominated domain suggests that hydrothermal chlorite was superimposed on previously sericitized and cemented felsic dominated breccia and that the chlorite alteration followed the second brecciation event.

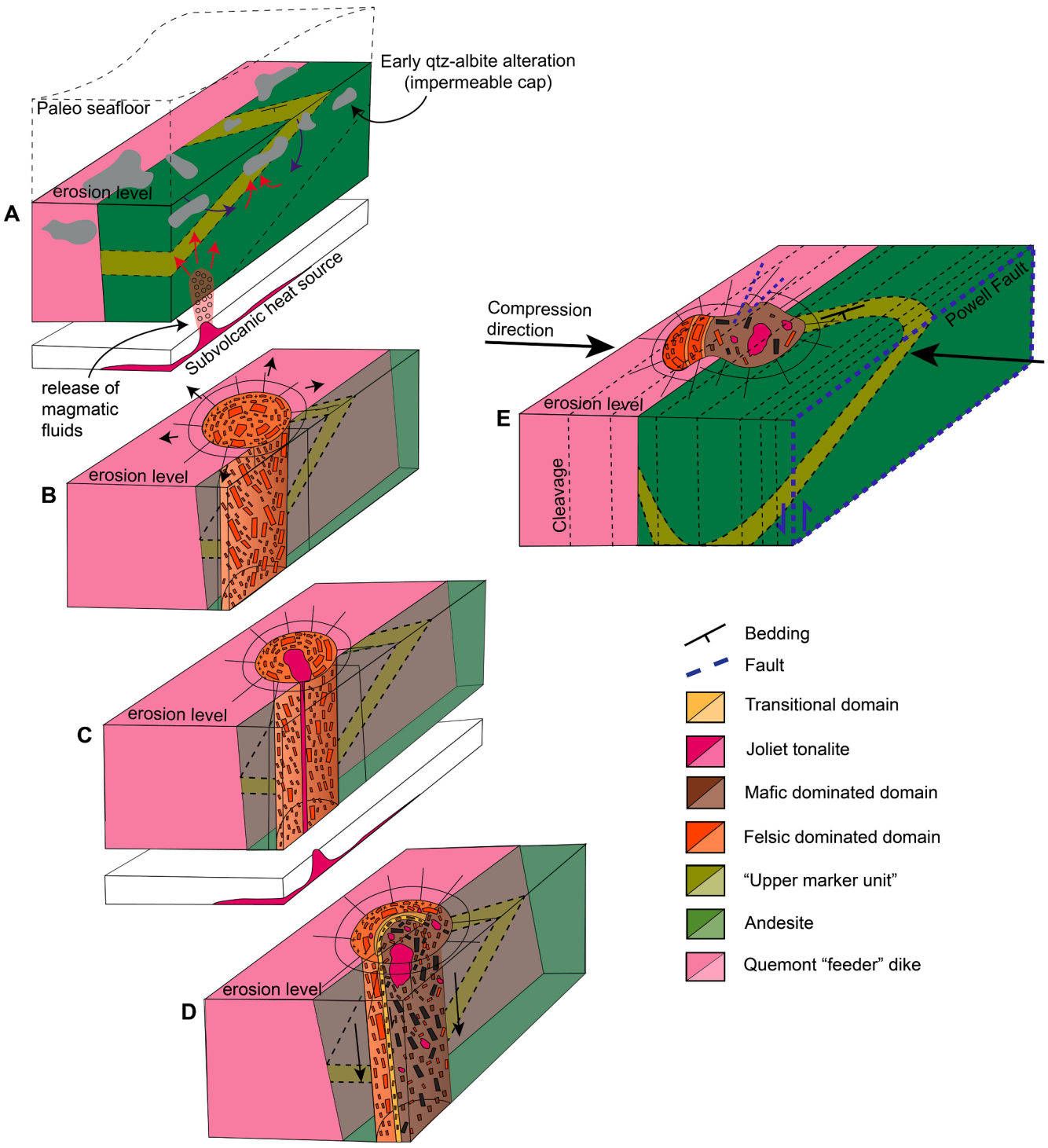

Fig. 11. Schematic diagram illustrating the interpreted model of formation of the Joliet Breccia, not to scale; A) Pre-breccia quartz-albite alteration may have reduced the permeability of the immediate host rocks; B) Catastrophic release of a magmatic fluid that became impounded, over pressured, and triggered a fragmentation event resulting in the formation of the felsic dominated domain; C) Intrusion of the Joliet Breccia tonalite; D) Second brecciation event and formation of the mafic dominated domain and associated chlorite alteration. Minor downward settling of breccia after fluid escapes and formation of the transitional domain. E) Current geometry of the Joliet Breccia after deformation. Colours match map legend from Fig. 3.

The compositional gains and losses attributed to chlorite and sericite alteration at the Joliet Breccia mimic those calculated by Riverin and Hodgson (1980) for the Millenbach VMS deposit within the Rouyn-Noranda mining district located a few km north of Joliet Breccia. Chlorite alteration is characterized by losses in Si, K, Na and Ca and gains in Fe. Similarly, spotted alteration is characterized by losses in Si, Na and Ca and gains in Al, K and Fe; sericite alteration shows Si and K gains and Na and Ca losses. The difference is Mg loss at the Joliet Breccia compared to Mg gain at Millenbach (supplementary data file 4; Fig. 9). The Fe/Mg ratio of chlorite is dominantly controlled by fluid composition, pH and temperature. The Mg content of chlorite in the upper parts of VMS systems is dominantly derived from interaction with seawater, whereas deeper upwelling hydrothermal fluids have a higher Fe/Mg ratio (Shikazono and Kawahata, 1987). Thus, VMS alteration pipes at Noranda are characterized

by an Fe-chlorite core grading upward and outward to Mg-chlorite and then sericite. The Millenbach samples reflect the Mg-rich chlorite present in the immediate sub-seafloor footwall rocks as opposed to the Joliet Breccia, which represents alteration within a deeper subsurface system.

The lateral and vertical zoning of alteration types, and metal tenor, as well as their timing is consistent with VMS footwall alteration zones at Noranda and elsewhere, with early quartz-albite alteration overprinted by an outer zone of sericite alteration and an inner chlorite alteration zone proximal to mineral occurrences and deposits (Riverin and Hodgson, 1980; Lesher et al., 1986; Maclean and Hoy, 1991; Franklin et al., 2005). In a VMS context, the quartz-albite alteration represents a semi-conformable alteration zone, which is interpreted to result from evolved seawater-rock interaction with down-welling modified seawater (Gibson et al., 1983). This laterally extensive alteration has been referred to as part of a self-sealing geothermal system at Noranda, wherein it served as an impermeable cap that focused subsequent VMS hydrothermal fluids to cross-cutting synvolcanic structures resulting in the superposition of discordant VMS alteration zones on regional quartz-albite alteration (Gibson et al., 1983). Thus, the lateral variation in alteration types within the Joliet Breccia may reflect a gradient in permeability, and likely temperature, with the highest water–rock ratio and temperature reflected by the internal chlorite alteration. This lateral zonation is also reflected in the Joliet Breccia metal tenors, with the highest values of Cu-Ag-Bi and Te located within the chlorite alteration of the mafic dominated domain. This metal zonation is typical of magmatic-hydrothermal deposits (Sillitoe, 2010) and VMS deposits due to the temperature dependent stability of CuCl complexes, wherein Cu becomes insoluble at temperatures <300 °C, which results in Cu mineralization being concentrated in the stockwork feeder zones and the base and interior of sulfide lenses (Lydon, 1988; Xiao et al., 1998; Franklin et al., 2005). In summary, the alteration mineralogy, attendant compositional changes and metal zonation are similar for the subsurface magmatic-hydrothermal Joliet Breccia and nearby seafloor VMS deposits, which may indicate similar fluid conditions and thus may further support a magmatic contribution to the VMS hydrothermal systems.

Wilson (1941) first noted the spotted-textured alteration in the Powell block and Lichtblau and Dimroth, (1980) and Lichtblau (1989), observed that it was particularly abundant within the Joliet Breccia. The clear fracture control of the spotted texture as haloes surrounding veins, and as rims surrounding clasts suggests a hydrothermal alteration origin. The spotted texture is similar to a well-known metamorphic texture within the Rouyn-Noranda mining district referred to as “dalmatianite” (De Rosen-Spence, 1969; Riverin and Hodgson, 1980), wherein cordierite porphyroblasts formed by contact metamorphism of Mg-altered mafic-intermediate volcanic rocks during intrusion of the ca. 2690 Ma post-volcanic Lac Dufault granitoid (Fig. 1). The cordierite porphyroblasts retrogressed to a subgreenschist facies mineral assemblage during regional metamorphism. The spotted-textured alteration in the Powell block is not associated with any known ca. 2690 Ma post-volcanic

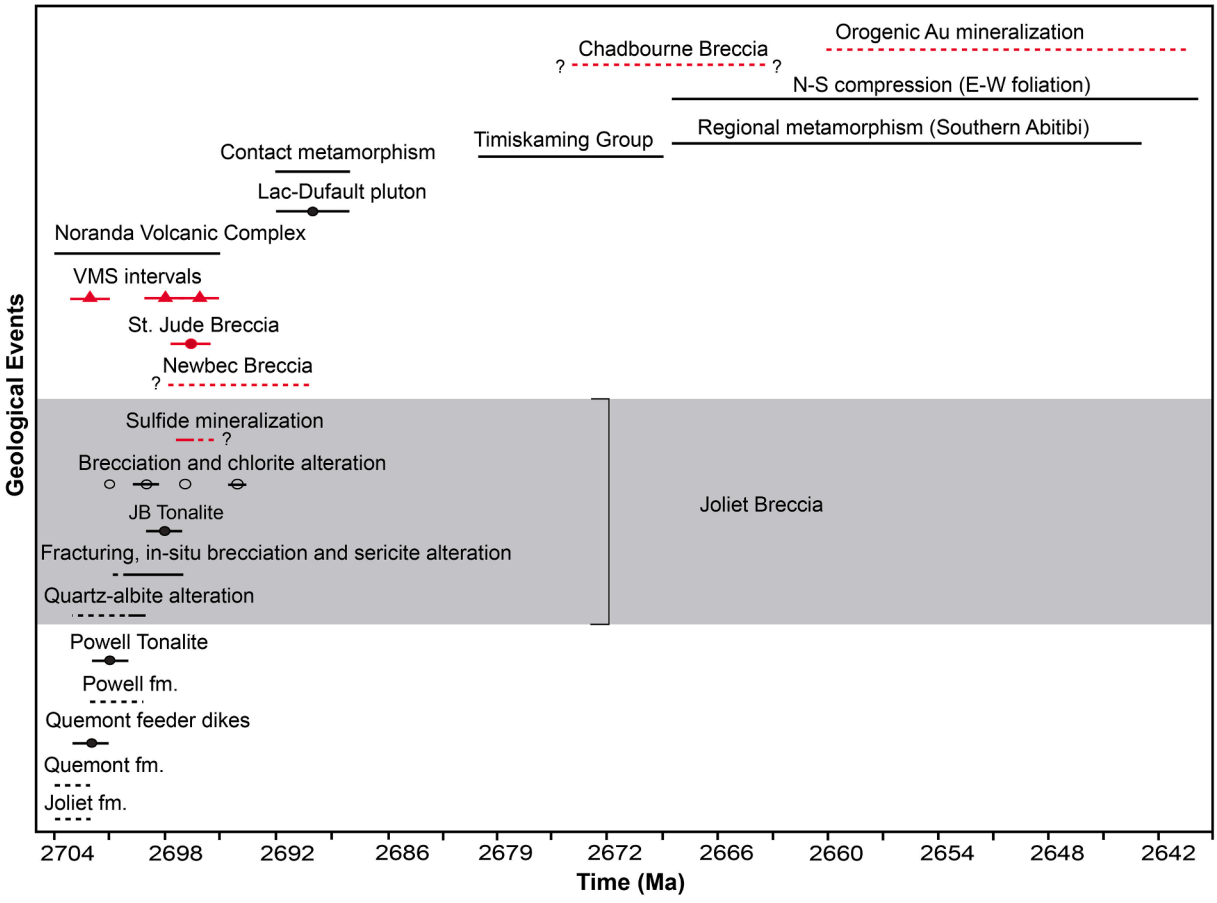

Fig. 12. Relative and absolute timing of the relevant major geological events. Shaded grey rectangle shows events occurring within the Joliet Breccia. Dashed lines are the projected possible age ranges. Black solid circles show zircon U-Pb TIMS ages. The four black hollow circles for brecciation and chlorite alteration within the Joliet Breccia show monazite U-Pb LA-ICP-MS ages from this study with the solid line showing the range within 2σ. The Powell tonalite and Joliet Breccia ages are from this study. St. Jude Breccia (Galley and Van Breemen, 2002). Newbec Breccia (Smith, 1983). Lac Dufault pluton (Mortensen, 1993). Quemont feeder dike, Noranda volcanic complex and VMS intervals (McNicoll et al., 2014). Contact metamorphism (De Rosen Spence, 1969; Mortensen, 1993). Chadbourne breccia (Walker and Cregheur, 1982). Regional deformation and gold mineralization in the Abitibi greenstone belt (Bedeaux et al., 2017; Wilkinson et al., 1999; Dubé and Mercier-Langevin, 2020) and regional metamorphism (Powell et al., 1995).

plutons, and if it is a retrogressed assemblage derived from an aluminosilicate porphyroblast, the precursor porphyroblast has not been identified. The spotted-texture alteration occurs in zones with a specific bulk composition, marked by gains in Rb, K, Ba, Mg and Fe and losses in Na and Ca, regardless of protolith, and appears to be geochemically intermediate between the sericite and chlorite alteration types. Therefore, the spotted texture is interpreted to represent either relict retrogressed porphyroblasts or new nodular chlorite-sericite intergrowths that preferentially developed in areas of intermediate alteration intensity.

5.5. Comparison to other known breccias within the Rouyn-Noranda mining district

The Joliet Breccia exhibits similarities to the Chadbourne, Newbec and St. Jude breccias (Fig. 1). The three breccia bodies and the Joliet Breccia are all spatially associated with intrusions, and are polymictic, with an abundance of andesitic blocks and variable proportions of felsic blocks. In addition, like the Joliet Breccia, the Chadbourne, and St. Jude breccias have: 1) gradational contacts with their host rocks, from an outer conjugate fracture set, to an incipient jig-saw fit breccia, to a rotated (±transported) matrix-clast supported breccia (Walker and Cregheur, 1982; Kennedy, 1985; Galley and van Breemen, 2002); 2) similar dimensions; and 3) a crudely elliptical morphology in plan view; the Newbec breccia has a triangular plan view (Smith, 1983). The key differences between these breccias are their matrix, metal content, and relative timing. The Joliet Breccia overlaps in time with the St. Jude breccia and possibly the Newbec breccia, however, the Chadbourne breccia is interpreted to be significantly younger (Fig. 12).

The Chadbourne breccia, one of the original discoveries in the camp, is an historic gold mine that produced 1.4 Mt of ore at a grade of 3.65 g/t Au. The breccia comprises andesitic blocks, with minor rhyolite blocks, in an open-space hydrothermal cement of quartz, albite, ankerite and dolomite with accessory pyrite, specularite and tourmaline. The timing of the Chadbourne breccia is poorly constrained. Walker and Cregheur (1982) suggested that the breccia was emplaced after the main regional post-Timiskaming (<2669 Ma) deformation, since the volcanic strata must have been tilted to steeper dips prior to emplacement. However, Dubé and Mercier-Langevin (2020), consider the Chadbourne breccia to have been emplaced pre-Timiskaming (>2669 Ma). The Chadbourne mineralization occurs within the open-space breccia matrix and consists of native Au and Ag, Au-telluride, as well as microscopic Au inclusions within pyrite, chalcopyrite, and galena and accessory magnetite (Walker and Cregheur, 1982). The mineralization is spatially associated with siliceous zones and is concentrated in cylindrical shoots with diameters up to 40 m that parallel the plunge of the breccia, which is typical of structurally controlled gold-mineralization, with gold following the dilatant zones (Walker and Cregheur, 1982). The Chadbourne breccia is spatially associated with a major fault zone and a pre- to early- Timiskaming age syenite intrusion, which was interpreted as a heat source and potential fluid source to drive hydrothermal circulation (Walker and Cregheur, 1982; Dubé and Mercier-Langevin, 2020).

The Newbec Breccia is a subeconomic Cu-Mo-Zn occurrence that contains subrounded-subangular fragments of diorite, andesite, quartz-feldspar porphyry, tuff, gabbro, and anorthositic gabbro in a matrix of fractured and chlorite altered quartz-feldspar porphyry ± pyrrhotite ± chalcopyrite ± pyrite ± molybdenite ± sphalerite (Smith, 1983). Locally the matrix is an open-space infill of crystalline quartz, chlorite, zoisite and ankerite (Smith, 1983). The timing of the Newbec breccia is poorly constrained. It was initially interpreted by Wilson (1941) as younger than the Lac Dufault intrusion due to the presence of angular fragments of granodiorite within the breccia adjacent to the contact. However, irregular offshoots of the granodiorite were observed to cross-cut the breccia leading Smith (1983) to interpret it as older than the Lac Dufault intrusion. The ~2690 Ma age for the Lac Dufault intrusion (Mortensen, 1993) makes the Newbec breccia pre-Timiskaming age. It was initially interpreted as a phreatic breccia that was overprinted by a magmatic brecciation event (Wilson, 1941). Smith (1983) interpreted the Newbec Breccia to have formed by a magmatic-hydrothermal fragmentation process.

The St. Jude Breccia, a subeconomic Au-Ag-Cu-Mo occurrence, comprises a polymictic breccia containing angular blocks of andesite wall-rock, and aphyric to porphyritic felsic intrusive blocks, in an igneous aplitic matrix (Galley and van Breemen, 2002). The brecciation event is bracketed by the age of the host trondjhemite phase of the Flavrian-Powell Intrusive Complex ca. 2700 + 3/-2 Ma and a cross-cutting quartz albite dike ca. 2696.6 ± 0.9 Ma (McNicoll et al., 2014) and is interpreted as ca. 2698 Ma (Galley and van Breemen, 2002). Its location on the margin of the synvolcanic Flavrian-Powell Intrusive Complex and spatial association with a small trondjhemite intrusion internal to the breccia suggests that it formed by a magmatic-hydrothermal fragmentation process (Galley and van Breemen, 2002). The trondjhemite intrusion is locally *in-situ* brecciated, and occurs as block sized clasts within the breccia (Galley and van Breemen, 2002). The St. Jude breccia is enriched in magmatophile (Ag, Te, Se, Bi, Sn) elements and exhibits a metal zonation with an internal Mo-rich zone and an outer Cu-rich zone, associated with a proximal biotite alteration and a distal sericite alteration, typical of high-temperature magmatic-hydrothermal mineralization (Kennedy, 1985; Galley and van Breemen, 2002).

The Joliet mine, hosted by rhyolite breccia, produced 1,465,403 t averaging 0.905% Cu, 8 g/t Ag, and 0.34 g/t Au (Sabina, 2003). Based on the ore outline displayed on historical company maps (Joliet-Quebec, 1948), at 100 m and 200 m depths, the orebody had a pipe-like shape with a diameter of 50 m and a long axis plunging moderately southward; however, it is now inaccessible and a detailed description of its mineralization and setting is lacking. The timing of the Joliet orebody is uncertain with the only age constraint being that it cross-cuts the Joliet Rhyolite, which is older than ca. 2702 Ma (McNicoll et al., 2014).

5.6. Metallogenic context of the Joliet Breccia within the Rouyn-Noranda mining district

Magmatism played a key role in the hydrothermal systems of the Rouyn-Noranda mining district, with VMS deposits forming at three intervals (ca. 2702 Ma, 2698–2697 Ma and 2696–2695 Ma) during the 7 m.y. interval of BRG volcanism that constructed the Noranda volcanic complex (McNicoll et al., 2014). The VMS deposits of the Noranda volcanic complex are enriched in magmatophile elements and the relative role of seawater and magmatic hydrothermal fluid in subseafloor VMS hydrothermal systems has been debated (Hannington et al., 1999; Franklin et al., 2005; Mercier-Langevin et al., 2011). Enrichment in magmatophile elements and Au at active hydrothermal vents on the seafloor (e.g., Brothers Volcano, Kermadec Arc, New Zealand; De Ronde et al., 2011; Susu Knolls, Manus Basin, Yeats et al., 2014) has been interpreted to indicate a magmatic fluid contribution to a seawater dominated hydrothermal system and similar arguments have been made for Au-enrichment at Horne and Quemont (Sharman et al., 2015; Krushnisky, 2018; Krushnisky et al., 2020). The Joliet Breccia, which is enriched in magmatophile elements, but Au poor, post-dates the nearby Au-rich Quemont and Horne VMS deposits (ca. 2702 Ma), but is temporally coincident with the youngest volcanic units (2696–2695 Ma) and VMS deposits of the Noranda Subgroup (McNicoll et al., 2014).

The brecciation mechanisms for the Joliet Breccia have been presented as separate models, but in reality they may represent a continuum. Phreatic breccias form in the cooler, distal near surface or seafloor portions of a deeper magmatic-hydrothermal system and subsurface magmatic-hydrothermal breccias themselves can grade downwards into igneous breccias (Lawless and White, 1990). Given the temporal overlap, the Joliet and St. Jude breccias and possibly the Newbec breccia (Fig. 12), may all be products of the same ca. 2698 Ma magmatic-hydrothermal event that formed VMS deposits at the seafloor and magmatic hydrothermal breccias at different crustal levels and in proximity to a magmatic source. This is consistent with more recent work in the Bergslagen district, Sweden,

where Allen et al. (1996), and Jansson and Allen (2011) invoked a continuum from deeper magmatic-hydrothermal processes to shallow VMS processes. In the Bergslagen and the Rouyn-Noranda mining districts the two systems became superimposed following burial and resurgent magmatic-hydrothermal processes resulting in the source intrusions and associated mineral deposits eventually cross-cutting older volcanic strata.

Thus, although the mineralized Joliet Breccia, St. Jude and Newbec breccias are not genetically or temporally related to their older host strata or to older VMS deposits, it does not preclude a potential indirect genetic association between these mineralized breccias and temporally correlated ca. $\leq$ 2698 Ma VMS deposits. These variably mineralized subsurface breccias may provide additional evidence for a magmatic contribution to the VMS hydrothermal system, as suggested by previous workers (Poulsen and Franklin, 1981; Walford and Franklin, 1982; Kennedy, 1985; Gibson and Watkinson, 1990; Poulsen and Hannington, 1996; Hannington et al., 1999; Franklin et al., 2005; Dubé et al., 2007; De Ronde et al., 2011; Huston et al., 2011). Thus, in ancient VMS districts an intimate association between magmatic-hydrothermal and VMS deposits should be expected, and this relationship may be analogous to that of the porphyry-epithermal continuum documented in modern subaerial arcs (Sillitoe, 2010).

The Chadbourne breccia exhibits many similarities to the Joliet, St. Jude and Newbec breccias, but its interpreted later timing suggests it is not temporally or genetically related. The Chadbourne breccia is most likely post-volcanic and pre-syn Timiskaming deformation (Fig. 12; Dubé and Mercier-Langevin, 2020).

6. Conclusions

The Joliet Breccia is a subsurface breccia, indicated by its discordant relationship, gradational contacts with wallrocks, and ca. 2698.9–2693 Ma age and is younger than the ca. <2702–2699.5 Ma volcanic units, and associated VMS deposits. However, the location of the Joliet Breccia to a synvolcanic structure, marked by the ca. 2702 Ma Quemont feeder dike, attests to the continued reactivation of fundamental structures during the evolution of the Noranda volcanic complex and its hydrothermal systems. Subseafloor magmatic-hydrothermal explosive processes account for the features observed within the Joliet Breccia and its contact and timing with the host rocks. Initial brecciation could have been triggered by a decrease in permeability due to early quartz-albite alteration and a build-up of hydrothermal fluid pressure during renewed magmatic-hydrothermal processes.

The timing for the Joliet Breccia overlaps with other brecciation and mineralization events within the Rouyn-Noranda mining district, including the St. Jude breccia and possibly the Newbec breccia, which are both Cu-Mo deposits spatially associated with intrusions. However, the key difference between these prospects and the Joliet Breccia is their magmatic matrix and/or high-temperature alteration assemblage, which is typical of some but not all magmatic-hydrothermal systems. The Joliet Breccia is interpreted to have formed at a shallower crustal level relative to the Newbec and St. Jude intrusive breccias. This suggests that localized ca. 2699–2695 Ma magmatic-hydrothermal events were superimposed on older volcanic strata, with variations in individual deposit characteristics reflecting differences in depth of formation and proximity to magmatic source. This new interpretation highlights the difficulty in recognizing and classifying subsurface breccia bodies, particularly in deformed and metamorphosed terranes, which can have important implications on metallogeny. Establishing discordance, contact relationships, as well as relative and absolute timing requires knowledge of the stratigraphy and structure of the volcanic succession, a fundamental requisite to recognizing subsurface breccias.

The lateral zoning of alteration types, compositional gains and losses, metal tenor and association, as well as their relative timing within the Joliet Breccia are similar to VMS footwall alteration zones at Noranda and elsewhere (Riverin and Hodgson, 1980; Lesher et al., 1986; Franklin et al., 2005). The VMS deposits hosted by the youngest units of the Blake River Group are broadly coeval with the timing of the St. Jude, Joliet and possibly Newbec breccias. Thus, within the context of the metallogeny of the larger Rouyn-Noranda mining district these breccias may be part of a broad continuum of subsurface magmatic-hydrothermal, and seafloor VMS deposits, akin to the porphyry-intermediate sulfidation epithermal continuum of modern subaerial volcanic arcs.

CRediT authorship contribution statement

Marina D. Schofield: Writing - original draft, Investigation, Data curation, Validation, Formal analysis, Visualization, Conceptualization. **Harold.L. Gibson:** Supervision, Funding acquisition, Writing - review & editing, Conceptualization. **Bruno Lafrance:** Supervision, Funding acquisition, Writing - review & editing, Conceptualization. **K. Howard Poulsen:** Supervision, Writing - review & editing, Conceptualization. **Jeffrey Marsh:** Investigation, Formal analysis, Data curation, Validation, Visualization, Writing - review & editing. **Michael A. Hamilton:** Investigation, Formal analysis, Data curation, Validation, Visualization, Writing - review & editing. **Taus R.C. Jørgensen:** Writing - review & editing.

Declaration of Competing Interest

The authors declare that they have no known competing financial interests or personal relationships that could have appeared to influence the work reported in this paper.

Acknowledgements

The authors extend much appreciation to Dr. Richard Sillitoe and Dr. Patrick Mercier-Langevin for their expertise and insight, which greatly improved the manuscript. Field assistant Mr. Michael Langa is thanked for eager, competent and able assistance in the field. Yorbeau Resources Inc. are thanked for allowing the use of their rock saw facilities during the field season. Dr. Gérald Riverin and Mr. Jean Goutier are thanked for providing critical historical data. Financial support was provided by Metal Earth though a Canada First Research Excellence Fund (CFREF) grant, which comprises a tri-agency initiative of the Natural Sciences and Engineering Research Council (NSERC), Social Sciences and Humanities Research Council (SSHRC), and the Canadian Institutes of Health Research (CIHR). Funding was also provided by federal, provincial, and industry partners of the Mineral Exploration Research Centre (MERC; http://merc.laurentian.ca/research/metal-earth/). This publication is a Metal Earth contribution MERC-ME-2020-102.

Appendix A. Supplementary data

Supplementary data to this article can be found online at https://doi.org/10.1016/j.precamres.2021.106264.

References

Allen, R.L., Lundstrom, I., Ripa, M., Simeonov, A., Christofferson, H., 1996. Facies analysis of a 1.9 Ga, continental margin, back-arc, felsic caldera province with diverse Zn-Pb-Ag-(Cu-Au) sulfide and Fe oxide deposits, Bergslagen region. Sweden. Econ. Geol. 91, 979–1008.

Allmendinger, R.W., Cardozo, N., Fisher, D., 2012. In: Structural Geology Algorithms: Vectors and Tensors. Cambridge University Press, Cambridge, p. 302.

Babcock, R.S., 1973. Computational models of metasomatic processes. Lithos 6 (3), 279–290.

Bedeaux, P., Pilote, P., Daigneault, R., Rafini, S., 2017. Synthesis of the structural evolution and associated gold mineralization of the Cadillac Fault, Abitibi, Canada. Ore Geol. Rev. 82, 49–69. https://doi.org/10.1016/j.oregeorev.2016.11.029.

Browne, P.R.L., Lawless, J.V., 2001. Characteristics of hydrothermal eruptions, with examples from New Zealand and elsewhere. Earth Sci. Rev. 52 (4), 299–331. https://doi.org/10.1016/S0012-8252(00)00030-1.

Camus, F., 1975. Geology of the El Teniente orebody with emphasis on wallrock alteration. Econ. Geol. 70, 1341–1372.

de Ronde, C.E.J., Massoth, G.J., Butterfield, D.A., Christenson, B.W., Ishibashi, J., Ditchburn, R.G., Hannington, M.D., Brathwaite, R.L., Lupton, J.E., Kamenetsky, V.S., Graham, I.J., Zellmer, G.F., Dziak, R.P., Embley, R.W., Dekov, V.M., Munnik, F.,

Lahr, J., Evans, L.J., Takai, K., 2011. Submarine hydrothermal activity and gold-rich mineralization at Brothers Volcano, Kermadec Arc, New Zealand. Miner. Deposita. 46 (5-6), 541–584. https://doi.org/10.1007/s00126-011-0345-8.
De Rosen-Spence, A., 1969. Genèse des roches à cordierite-anthophyllite des gisements cupro-zincifères de la région de Rouyn-Noranda, Québec, Canada. Can. J. Earth Sci. 6, 1339–1345.
De Rosen Spence, A.F., 1976. Stratigraphy, Development and petrogenesis of the central Noranda volcanic pile, Noranda, Québec. PhD thesis. University of Toronto, Toronto, Ontario.
Dimroth, E., Rocheleau, M., 1979. Volcanology and Sedimentology of Rouyn-Noranda Area, Québec, in: Geological Association of Canada and Mineralogical Association of Canada Field Trip A-1 Guidebook. Université Laval, Québec, pp. 111–125.
Dimroth, E., Imreh, L., Goulet, N., Rocheleau, M., 1983. Evolution of the south-central segment of the Archean Abitibi Belt, Québec. Part II: Tectonic evolution and geomechanical model. Can. J. Earth. Sci. 20, 1355–1373.
Dubé, B., Mercier-Langevin, P., Hannington, M.D., Lafrance, B., Gosselin, G., Gosselin, P., 2007. The Laronde Penna Au-rich volcanogenic massive sulfide deposit, Abitibi Greenstone Belt, Québec: mineralogy and geochemistry of alteration and implications for genesis and exploration. Econ. Geol. 102, 633–666.
Dubé, B., Mercier-Langevin, P., 2020. Gold deposits of the Archean Abitibi Greenstone belt, Canada. In: Sillitoe, R.H., Goldfard, R.J., Robert, F., Simmons, S.F. (Eds.), Geology of the world's major gold deposits and provinces, SEG Special Publication, pp. 669–708.
Einaudi, M.T., Hedenquist, J.W., Inan, E.E., 2003. Sulfidation state of fluids in active and extinct hydrothermal systems: transitions from porphyry to epithermal environments. In: SEG Special Publication, pp. 285–314.
Fisher, R.V., Schmincke, H.U., 1984. In: Pyroclastic Rocks. Springer, Berlin Heidelberg, Berlin, Heidelberg. https://doi.org/10.1007/978-3-642-74864-6.
Franklin, J.M., Gibson, H.L., Jonasson, I.R., Galley, A.G., 2005. In: Volcanogenic Massive Sulfide Deposits. Econ. Geol. 100th Anniv., pp. 523–560.
Galley, A., Breemen, O.v., Franklin, J., 2000. The relationship between intrusion-hosted Cu-Mo mineralization and the VMS deposits of the Archean Sturgeon Lake mining camp, Northwestern Ontario. Econ. Geol. 95 (7), 1543–1550. https://doi.org/10.2113/gsecongeo.95.7.1543.
Galley, A.G., van Breemen, O., 2002. Timing of synvolcanic magmatism in relation to base-metal mineralization, Rouyn-Noranda, Abitibi volcanic belt, Québec. Geol. Surv. Canada Curr. Res.
Gibson, H.L., 1990. The mine sequence of the Central Noranda volcanic complex: geology, alteration, massive sulfide deposits and volcanological reconstruction. Ph. D. thesis. Carleton University, Ottawa, Ontario.
Gibson, H.L., Watkinson, D.H., 1990. Volcanogenic Massive Sulphide Deposits of the Noranda Cauldron and Shield Volcano, Québec. Can. Inst. Min. Metall. Spec. 43, 119–132.
Gibson, H.L., 2005. Chapter 12 Volcanic-hosted ore deposits. In: Martí, J., Ernst, G. (Eds.), Volcanoes and the Environment. Cambridge University Press, pp. 333–386.
Gibson, H.L., Watkinson, D.H., Comba, C.D.A., 1983. Silicification: hydrothermal alteration in an Archean geothermal system within the Amulet rhyolite formation, Noranda, Québec. Econ. Geol. 78, 954–971. https://doi.org/10.2113/gsecongeo.78.5.954.
Gilligan, L.B., Marshall, B., 1987. Textural evidence for remobilization in metamorphic environments. Ore Geol. Rev. 2 (1-3), 205–229. https://doi.org/10.1016/0169-1368(87)90029-1.
Goodwin, A.M., 1980. Archean volcanic studies in the Timmins-Kirkland Lake-Noranda region of Ontario and Québec. Can. Geol. Surv. Bull. 278 https://doi.org/10.4095/106237.
Goulet, N., 1978. Stratigraphy and structural relationships across the Cadillac – Larder Lake Fault, Rouyn – Beauchastel area, Québec. PhD thesis. Queen's University, Kingston, Ontario.
Gresens, R.L., 1967. Composition-volume relationships of metasomatism. Chem. Geol. 2, 47–65.
Hannington, M.D., Poulsen, K.H., Thompson, J.F.H., Sillitoe, R.H., 1999. Volcanogenic gold in the massive sulfide environment. In: Barrie, C.T., Hannington, M.D. (Eds.), Volcanic-Associated Massive Sulfide Deposits: Processes and Examples in Modern and Ancient Settings. Reviews in Economic Geology, pp. 325–356.
Hart, T.R., Gibson, H.L., Lesher, C.M., 2004. Trace element geochemistry and petrogenesis of felsic volcanic rocks associated with volcanogenic massive Cu-Zn-Pb sulfide deposits. Econ. Geol. 99 (5), 1003–1013.
Hitzman, M.W., 1999. Routine staining of drillcore to determine carbonate mineralogy and distinguish carbonate alteration textures. Miner. Deposita 34 (8), 794–798.
Horstwood, M.S.A., Košler, J., Gehrels, G., Jackson, S.E., McLean, N.M., Paton, C., Pearson, N.J., Sircombe, K., Sylvester, P., Vermeesch, P., Bowring, J.F., Condon, D.J., Schoene, B., 2016. Community-derived standards for LA-ICP-MS U-(Th-) Pb geochronology–Uncertainty propagation, age interpretation and data reporting, Geostand. Geoanal. Res. 40 (3), 311–332.
Hubert, C., Trudel, P., Gélinas, L., 1984. Archean wrench fault tectonics and structural evolution of the Blake River Group, Abitibi belt, Québec. Can J. Earth Sci. 21, 1024–1032.
Huston, D.L., Relvas, J.M.R.S., Gemmell, J.B., Drieberg, S., 2011. The role of granites in volcanic-hosted massive sulphide ore-forming systems: an assessment of magmatic – hydrothermal contributions. Miner. Deposita 46, 473–507. https://doi.org/10.1007/s00126-010-0322-7.
Jaffey, A.H., Flynn, K.F., Glendenin, L.E., Bentley, W.C., Essling, A.M., 1971. Precision measurement of half-lives and specific activities of 235U and 238U. Phys. Rev. 4, 1889–1906.
Jansson, N.F., Allen, R.L., 2011. Timing of volcanism, hydrothermal alteration and ore formation at Garpenberg, Bergslagen, Sweden. Geol. Foeren. Stockholm Foerh. 133 (1-2), 3–18. https://doi.org/10.1080/11035897.2010.547597.
Jébrak, M., 1997. Hydrothermal breccias in vein-type ore deposits: a review of mechanisms, morphology and size distribution. Ore Geol. Rev. 12 (3), 111–134.
Joliet-Quebec Mines Ltd. 1948. Plan of surface geology and drilling, Rouyn Twp., N.W. Quebec, unpublished geological map, 1 sheet, one inch to 200 feet.
Katz, L.R., Kontak, D.J., Dubé, B., McNicoll, V., 2017. The geology, petrology, and geochronology of the Archean Coté Gold large-tonnage, low-grade intrusion-related Au(-Cu) deposit, Swayze greenstone belt, Ontario Canada. Can. J. Earth Sci. 54, 173–202. https://doi.org/10.1139/cjes-2016-0007.
Kennedy, L.P., 1985. The geology and geochemistry of the Archean Flavrian pluton, Noranda, Québec. The University of Western Ontario. PhD thesis.
Koide, H., Bhattarcharji, S., 1975. Formation of fractures around magmatic intrusions and their role in ore localization. Econ. Geol. 70, 781–799.
Krushnisky, A., 2018. Controls of gold enrichment at the Horne 5 Archean VMS deposit, Abitibi greenstone belt, Québec. MSc thesis. Institut national de la recherche scientifique – Centre Eau Terre Environment, Québec City, Québec.
Krushnisky, A., Mercier-Langevin, P., Ross, P.S., Goutier, J., Pilote, C., Bernier, C., 2020. Geology and gold enrichment at the Horne 5 Archean volcanogenic massive sulpide deposit, Abitibi greenstone belt, Québec: a synthesis. In: Mercier-Langevin, P., Lawley, C.J.M., Castonguay, S. (Eds.), Targeted Geoscience Initiative 5: Contributions to the Understanding of Canadian Gold Systems, pp. 31–44. https://doi.org/10.4095/323663.
Lawless, J.V., White, P.J., 1990. Ore-related breccias: a revised genetical classification with particular reference to epithermal deposits. In: 12th New Zealand Geothermal Workshop, pp. 197–202.
Lesher, C.M., Gibson, H.L., Campbell, I.H., 1986. Composition-volume changes during hydrothermal alteration of andesite at Buttercup Hill, Noranda District, Québec. Geochim. Cosmochim. Acta 50, 2693–2705. https://doi.org/10.1016/0016-7037(86)90219-X.
Lichtblau, A., 1989. Stratigraphy and Facies at the south margin of the Archean Noranda Caldera. MSc thesis. l'Université du Québec à Chicoutimi, Chicoutimi, Québec.
Lichtblau, A., Dimroth, E., 1980. Stratigraphy and facies at the South margin, of the Archean Noranda Caldera, Noranda, Québec. Geol. Surv. Canada Curr. Res. Part A 69–76.
Lorenz, V., 1973. On the formation of maars. Bull. Volcanol. 37 (2), 183–204.
Lydon, J.W., 1988. Ore deposit models: Volcanogenic massive sulfide deposits. Part 1: a descriptive model. Geosci. Can. 11, 195–202.
Maclean, W.H., Hoy, L.D., 1991. Geochemistry of hydrothermally altered rocks at the Horne Mine, Noranda, Québec. Econ. Geol. 86, 506–528. https://doi.org/10.2113/gsecongeo.86.3.506.
Mathieu, L., Racicot, D., 2019. Petrogenetic study of the multiphase chibougamau pluton: Archaean magmas associated with Cu-Au magmato-hydrothermal systems. Minerals 9 (3), 174. https://doi.org/10.3390/min9030174.
Mercier-Langevin, P., Hannington, M.D., Dubé, B., Bécu, V., 2011. The gold content of volcanogenic massive sulfide deposits. Miner. Depos. 46 (5-6), 509–539. https://doi.org/10.1007/s00126-010-0300-0.
McNicoll, V., Goutier, J., Dubé, B., Mercier-Langevin, P., Ross, P.S., Dion, C., Monceck, T., Legault, M., Percival, J., Gibson, H., 2014. U-Pb geochronology of the Blake River Group, Abitibi greenstone belt, Québec, and implications for base metal exploration. Econ. Geol. 109, 27–59. https://doi.org/10.2113/econgeo.109.1.27.
Mitcham, T., 1974. Origin of breccia pipes. Econ. Geol. 69, 412–413.
Morris, H. R. 1957. Héré Fault Copper Ltd. Surface Geology, Anglo-Rouyn and North Part of Powell-Rouyn properties, Rouyn Twp., N.W. Québec, unpublished geological map, 3 sheets, one inch to 200 feet.
Morris, H.R., 1959. Joliet-Québec Mines Ltd. Surface Geology, Rouyn Twp., N.W. Québec, unpublished geological map, 3 sheets, one inch to 200 feet.
Mortensen, J.K., 1993. U-Pb geochronology of the eastern Abitibi subprovince. Part 2. Noranda-Kirkland Lake area. Can J. Earth. Sci. 30 (1), 29–41.
Muffler, L.J.P., White, D.E., Truesdell, A.H., 1971. Hydrothermal explosion craters in Yellowstone National Park. Geol. Soc. Am. Bull. 82 (3), 723. https://doi.org/10.1130/0016-7606(1971)82[723:HECIYN]2.0.CO;2.
Pearce, J.A., 1996. A user's guide to basalt discrimination diagrams, in: Bailes, A.H. (Eds.), Trace Element Geochemistry of Volcanic Rocks: Applications for Massive Sulfide Exploration. Geological Association of Canada, Short Course Notes, 12pp. 79-113.
Poulsen, K.H., 2017. Chapter 5 The Larder Lake-Cadillac Break and Its Gold Districts. In: Monecke, T., Mercier-Langevin, P., Dubé, B. (Eds.), Archean Base and Precious Metal Deposits, Southern Abitibi Greenstone Belt, Canada. Reviews in Economic Geology, pp. 133–167.
Poulsen, K.H., Franklin, J.M., 1981. Copper and gold mineralization in an Archean trondjhemitic intrusion Sturgeon Lake, Ontario. In: Current Research Part A. Geological Survey of Canada, pp. 9–14.
Poulsen, K.H., Hannington, M.D., 1996. Volcanic-associated massive sulphide gold. In: Eckstrand, R.O., Sinclair, W.D., Thorpe, R.I. (Eds.), Geology of Canadian Mineral Deposit Types, pp. 183–196.
Powell, W.G., Carmichael, D.M., Hodgson, C.J., 1995. Conditions and timing of metamorphism in the southern Abitibi Greenstone Belt, Québec. Can. J. Earth Sci. 32, 787–805. https://doi.org/10.1139/e95-067.
Reynolds, D.L., 1954. Fluidization as a geological process, and its bearing on the problem of intrusive granites. Am. J. Sci. 252 (10), 577–613. https://doi.org/10.2475/ajs.252.10.577.
Riverin, G., Hodgson, C.J., 1980. Wall-rock alteration at the Millenbach Cu-Zn mine, Noranda, Québec. Econ. Geol. 75, 424–444. https://doi.org/10.2113/gsecongeo.75.3.424.

Ross, P.-S., Bédard, J.H., 2009. Magmatic affinity of modern and ancient subalkaline volcanic rocks determined from trace-element discriminant diagrams. Can J. Earth Sci. 46 (11), 823–839. https://doi.org/10.1139/E09-054.
Sabina, A.P., 2003. Rocks and minerals for the collector: Kirkland Lake-Rouyn-Noranda-Val d'Or, Ontario and Québec. In: Geological Survey of Canada, Miscellaneous Report, p. 322.
Sawkins, F.J., 1990. In: Metal Deposits in Relation to Plate Tectonics, second ed. Springer-Verlag, Berlin Heidelberg, p. 461. https://doi.org/10.1007/978-3-662-08681-0.
Sharman, E.R., Taylor, B.E., Minarik, W.G., Dubé, B., Wing, B.A., 2015. Sulfur isotope and trace element data from ore sulfides in the Noranda district (Abitibi, Canada): implications for volcanogenic massive sulfide deposit genesis. Miner. Deposita 50 (5), 591–606. https://doi.org/10.1007/s00126-014-0559-7.
Shikazono, N., Kawahata, H., 1987. Compositional differences in chlorite from hydrothermally altered rocks and hydrothermal ore deposits. Can. Mineral. 25 (3), 465–474.
Sibson, R.H., 1986. Brecciation processes in fault zones: Inferences from earthquake rupturing. Pure Appl. Geophys. 124 (1-2), 159–175.
Sillitoe, R.H., Sawkins, F.J., 1971. Geologic, Mineralogic and Fluid Inclusion Studies Relating to the Origin of Copper-bearing Tourmaline Breccia Pipes, Chile. Econ. Geol. 66, 1028–1041.
Sillitoe, R.H., 1985. Ore-Related Breccias in Volcanoplutonic Arcs. Econ. Geol. 80, 1467–1514.
Sillitoe, R.H., 2010. Porphyry copper systems. Econ. Geol. 105 (1), 3–41. https://doi.org/10.2113/gsecongeo.105.1.3.
Smith, W.K., 1983. A Petrographic Description of the Newbec Breccia, Noranda, Quebec. BSc thesis. University of Waterloo, Waterloo, Ontario.
Sun, S.S., McDonough, W.F., 1989. Chemical and isotopic systematics of oceanic basalts: implications for mantle composition and processes. In: Saunders, A.D., Norry, M.J. (Eds.), Magmatism and ocean basins. Geol. Soc. Lond., pp. 313–345.
Tosdal, R.M., Richards, J.P., 2001. Chapter 6 Magmatic and Structural Controls on the Development of Porphyry Cu ± Mo ± Au Deposits. In: Richards, J.P., Tosdal, R.M. (Eds.), Structural Controls on Ore Genesis. Reviews in Economic Geology, pp. 157–181.
Walford, P.C., Franklin, J.M., 1982. The Anderson Lake Mine, Snow Lake, Manitoba. In: Hutchinson, R.W., Franklin, J.M. (Eds.), Precambrian sulphide deposits. Geol. Assoc. Can. Spec. Pap., pp. 481–523.
Walker, S.D., Cregheur, P., 1982. The Chadbourne Mine, Noranda, Quebec: A gold-bearing breccia. In: Hodder, R.W., Petruk, W. (Eds.), Geology of Canadian Gold Deposits. Canadian Institute of Mining and Metallurgy, pp. 58–66.
White, J.D.L., Ross, P.-S., 2011. Maar-diatreme volcanoes: a review. J. Volcanol. Geotherm. Res. 201 (1-4), 1–29.
Wilkinson, L., Cruden, A.R., Krogh, T.E., 1999. Timing and kinematics of post-Timiskaming deformation within the Larder Lake - Cadillac deformation zone, southwest Abitibi greenstone belt, Ontario, Canada. Can. J. Earth Sci. 36 (4), 627–647. https://doi.org/10.1139/e99-015.
Wilson, M.E., 1941. Noranda district, Québec. Geological Survey of Canada. Memoir 229, 162 p. https://doi.org/10.4095/101612.
Woodcock, N.H., Mort, K., 2008. Classification of fault breccias and related fault rocks. Geol. Mag. 145 (3), 435–440. https://doi.org/10.1017/S0016756808004883.
Xiao, Z., Gammons, C.H., Williams-Jones, A.E., 1998. Experimental study of copper (I) chloride complexing in hydrothermal solutions at 40-300C and saturated water vapor pressure. Geochemica Cosmochim. Acta 62, 2949–2964.
Yeats, C.J., Parr, J.M., Binns, R.A., Gemmell, J.B., Scott, S.D., 2014. The SuSu Knolls hydrothermal field, eastern Manus Basin, Papua New Guinea: an active submarine high-sulfidation copper-gold system. Econ. Geol. 109 (8), 2207–2226.